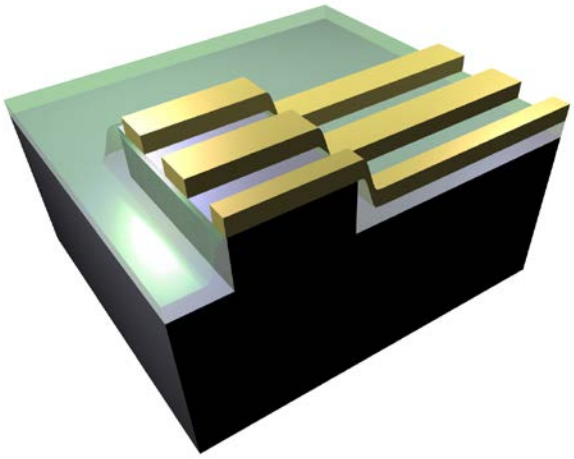
# Studies of Magnetoresistance and Hall Sensors in Semiconductors



**Praphaphan Noom Wipatawit**

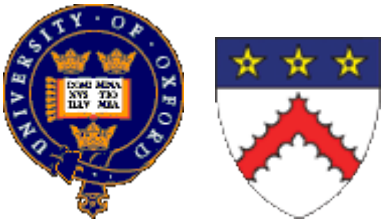
**Keble College**
**University of Oxford**

**A thesis submitted for the degree of**

***Doctor of Philosophy***

**Hilary 2006**

# Studies of Magnetoresistance and Hall Sensors in Semiconductors



**Praphaphan Noom Wipatawit**

**Keble College**
**University of Oxford**

**A thesis submitted for the degree of**

***Doctor of Philosophy***

**Hilary 2006**

# Studies of Magnetoresistance and Hall Sensors in Semiconductors

Praphaphan Noom Wipatawit
Keble College.

A thesis submitted for the Degree of Doctor of Philosophy
Hilary term 2006

## Abstract

The design, fabrication and performance of an Extraordinary Magnetoresistance (EMR) and a Vertical Mesa Hall Sensor (VMHS) are studied.

EMR devices have been fabricated from a 2DEG InAs/GaSb structures which exhibit a low carrier density and high mobility that achieve the best performance. The general electrical magneto-transport properties are given. The experiments investigate mainly different metallic patterns, which are Rectangular, Triangular and Tip pattern between 4-300 K. Probe configurations and the enhancement of relative size of metallic patterns are described. EMR effect is due to current deflection around the metal-semiconductor interface. The results are metallic pattern dependent. Using finite element analysis, good agreement between experimental and theoretical results was found. The best performance sensor is a symmetrical metallic Tip pattern. It is enhanced by the length of the Tip's point and the large metallic area. This pattern when combines with an asymmetrical probe configuration, exhibits the highest EMR of 900% at –0.275T measured by inner probes and the best sensitivity of 54Ω/T at room temperature.

The second study presents in-plane Hall effect sensors made from InSb. A simple device geometry has been used in which current flows in a plane perpendicular to the device surface. Device sensitivity depends on its geometry and a series of different contacts are used to investigate the geometry of the current flow distribution. The structures produced are only sensitive to the presence of one in-plane field component, and they also demonstrate good angular selectivity. Multi-electrodes were used to investigate biasing current from both mesa and substrate condition. We are able to examine the Hall voltage as a function of contact positions and also to create multiple VMHS. Offset reduction of devices has been achieved by moving the ground contacts to re-balance the current distribution under the mesa surface.

# Acknowledgements

I would like to thank all those who have helped in the preparation of this thesis, in particular:

Prof. R.A. Cowley and Prof. J.F. Ryan for extending to me the facilities of the Clarendon Laboratory.

My supervisor, Prof. Robin Nicholas for his encouragement, enthusiasm and guidance over the last four years.

Dr. N. J. Mason and Dr. P. Shields for growing many of the samples that are studies in this thesis. Dr. C. Goodwin for advising to thin film technology.

My research colleagues: Kei Takashina for his help in many experiments and tutor to superconducting magnet, Vicky Broadley for introducing me to fabrication process in cleanroom, Cattleya Petchshngh, Beata Kardynal, Gavin Cobineer. Tim Stadelmann for excellent LABVIEW program and any valuable discussion, Chris Bumby for etching process and introduce me to any sports he can play. Greg Wiltshire, Russel Deacan, James Doig for reading my thesis, Edouard Alphandery, Rizwan Chugtai, Victor Zhitomirsky, Lance Li, Ian Mortimer, Ben Nedniyom, Adrian Nish. Special thanks to Mrs Hillary Pyes for checking my English grammar and also Mr Ufuk Yilmas for reading my thesis and also valuable tea time discussion.

The technical staff at the laboratory, Darren Wallace, especially Keith Belcher for his provision of and extremely convenient working table and constant assistance,

Finally, I would like to dedicate this thesis to my Papa, May, Nui and friends for their unending support and encouragement that I can never thank enough.

# Contents


## Part I Magnetoresistance Sensors

**1.Introduction 2**

1.1 Galvanomagnetic effects……..……...4

*1.1.1 Lorentz Force*…….……4

*1.1.2 Magnetoresistivity Tensor*……..…..……7

1.2 The shape of semiconductors and electrodes used in Hall devices…….8

1.3 Extraordinary Magnetoresistance…….….12

1.4 Bilinear Transformation……...…….14

1.5 Review of current EMR structure and materials……..…….17

1.6 Geometry of the samples ……..22

1.7 GaSb/InAs/GaSb Heterostructures ……..…….……24

**2. Experimental Techniques and Device Fabrication 31**

2.1. Introduction……..……..31

2.2. Growth Techniques……..……..31

2.3. Device Fabrication……..……...32

2.4. Measurement…… 35

*2.4.1 The calibration of the vdP Hall sensors.*……..…..…..…

**3. The Influence of geometry with various metallic patterns 43**

3.1 Rectangular metallic pattern: (Type I) ……...…….45

*3.1.1 The Enhancement of magnetoresistance*…….……45

*3.1.2 Probe configuration*……47

*3.1.3 Experimental and computed results*…...……49

3.2 Triangular metallic Pattern: (Type II) …….……57

*3.2.1 Experimental samples*……..……..…..…57

*3.2.2 Computed samples*……...……..…….58

*3.2.3 Probe configuration*……59

*3.2.4 Experimental and computed results*…...……59

3.3 Metallic tip pattern: (Type III)…….66

*3.3.1 Samples*……...……...……..…67

*3.3.2 Probe configuration*……68

*3.3.3 Experimental and computed results*……68

3.4 Others Metallic patterns and their results……...……...……...78

*3.4.1 Plus-shaped metallic pattern*……..……78

*3.4.2 Needle metallic pattern*……....……...80

*3.4.3 L-shaped metallic pattern*……..…….81

*3.4.4 Meander metallic pattern*……..…….....83

3.5 Temperature dependence…….…..……84

*3.5.1 Rectangular metallic pattern*…….…….86

*3.5.2 Triangular metallic pattern*…….…..…..89

*3.5.3 Metallic tip pattern*……..…...90

3.6 Summary…….…..…91

3.7 References……...…….93

**4 The Influence of geometry and Conclusions 95**

4.1 The extraordinary magnetoresistance and the sensitivities of samples……95

4.2 Devices applications ……...……..…99

4.3 References……...…….…..103

**Part II Vertical Hall Sensors**

**5. Introduction 105**

5.1 Introduction…….…..……...…105

5.2 Materials and Technology……..……106

5.3 Basic physical consideration…….…….106

*5.3.1 Hall Voltage*……..……..107

*5.3.2 Offset*……..……108

*5.3.3 Sensitivity*……..…….109

5.4 Interpretation……..110

5.5 References……..112

**6. Design consideration and Fabrication 114**

6.1 Design consideration……..115

6.2 Fabrication Process…….116

6.3 Samples……..119

6.4 Measurement……..120

*6.4.1 Hall voltage*……...……121

*6.4.2 Current dependence*…….……122

*6.4.3 Angular dependence*……122

6.5 References…….…….123

**7. Experimental results 125**

7.1 Simple 3-electrode structures…….……126

*7.1.1 In-plane measurement*…….…126

*7.1.2 Current dependence*……..…128

*7.1.3 Angular Field dependence*…….……...……129

*7.1.4 Summary of the sensitivities of the VMHS*….……..……130

7.2 Multiple electrodes Concept……...….……..135

*7.2.1 The Hall voltage as a function of contact positions*……..……...….135

*7.2.1.1 Substrate bias (VMHSs)*……...…135

*7.2.1.2 Mesa Bias (VMHSm)*……139

*7.2.1.3 Discussion*……..……...……142

*7.2.2 Multiple VMHS on a single mesa*……...……143

*7.2.2.1 Substrate bias (VMHSs)*……144

*7.2.2.2. Mesa Bias (VMHSm)*……145

7.3 Multiple contacts and offset reduction……...147

7.4 Conclusions……151

7.5 References……..154

**8. Summary of the thesis and future works 156**

8. Summary of the thesis and future works…..…….157

8.1 Summary the accomplishment of the devices……..……....157

8.2 Future works...……...160

8.3 References……161

# Part I Magnetoresistance sensors.

# Chapter 1

# Introduction

1.1 Galvanomagnetic effects……..……...4

*1.1.1 Lorentz Force*…….……4

*1.1.2 Magnetoresistivity Tensor*……..…..……7

1.2 The shape of semiconductors and electrodes used in Hall devices…….8

1.3 Extraordinary Magnetoresistance…….….12

1.4 Bilinear Transformation……...…….14

1.5 Review of current EMR structure and materials……..…….17

1.6 Geometry of the samples ……..22

1.7 GaSb/InAs/GaSb Heterostructures ……..…….……24

1.8 References……..26

# Part I Magnetoresistance sensors

## 1.Introduction

A magnetic sensor is a transducer that converts a magnetic field into an electrical signal. Semiconductor magnetic sensors exploit the galvanomagnetic effect arising due to the Lorentz force on charge carriers. These effects occur when a material carries an electric current in the presence of a magnetic field. There are two galvanomagnetic effects in a semiconductor system, the Hall effect and the magnetoresistance effect.

Hall effect devices, such as the Hall cross and geometric magnetoresistor, are magnetic field sensors based on the classical Hall effect. Recently, Hall devices have been used in a wide range of applications[1-7] as they produce the linearity of magnetic response. Moreover, they can be used in an industrial environment because of their robustness, insensitivity to dirt, and suitability for remote sensing. They have also become a popular for a magnetic recording media.[8]

Magnetoresistance (MR) effect is a general term for the changes the resistivity of a material. In 1980, a new form of this effect called “Giant magnetoresistance” (GMR)[9-14] was discovered in magnetic multilayer structures. Most GMR devices contain alternating layers of a magnetic element and a non-magnetic element. Initially, multilayer devices were produced using molecular beam epitaxy (MBE) that approaches perfect crystals with sharp interfaces between the layers. However, it is still expensive and more complicated than other growth methods.

The two main disadvantages of the GMR sensor are the flipping effect and hysteresis. In the manufacture process, GMR sensors have to be magnetized in the direction of the layers. If this magnetization is disturbed by a large opposite field, the characteristics of the sensor may be either distorted or reversed (flipped).[15]

In non-magnetic semiconductors, the magnetoresistance effect results from two contributing effects: intrinsic (physical) MR and geometrical MR. Physical MR comes from the physical properties of material such as the charge mobility, while geometrical MR is related to the change of the current path in a specific sample geometry. Geometrical MR increases quadratically with charge mobility and magnetic field (at low field). Therefore, high mobility semiconductors such as InSb and InAs are attractive materials for experiments that explore geometrical effects.

Furthermore, it has been found that inhomogeneous semiconductor devices with metallic inclusions embedded inside the semiconductor material can show enhanced MR,[16] called Extraordinary Magnetoresistance (EMR).[17] Recently, Solin and co-workers at NEC and Ohio University took a very different approach by exploiting geometrical aspects of Extraordinary Magnetoresistance (EMR) using structures including an 'external metallic shunt'.[17]

Part I of this thesis uses a room temperature high mobility 2D electron system very close to the surface of the semiconductor and the study of new geometries to investigate enhancement of the magnetoresistance properties. The devices used in the experimental work employ an InAs/GaSb double heterostructure system, which is known to have a type II broken gap band alignment.[18] Our studies concern the electrical properties of devices of both

symmetric and asymmetric structures.

This chapter reviews the background of Extraordinary Magnetoresistance and shows that device geometry can significantly enhance the ordinary magnetoresistance effect. Discussion of a simplified model of the Hall effect leads to a more detailed analysis of our sample geometries. Basic properties of the material are described, and relevant aspects of the GaSb/InAs/GaSb heterostructure system are briefly reviewed.

## 1.1 Galvanomagnetic effects

In order to understand the background of the magnetoresistance effect a brief description of the physical effects basic to operation of magnetoresistance devices will be given. Since all galvanomagnetic effects come from the Lorentz forces, these are discussed first.

### 1.1.1 Lorentz Force

When we apply an electric field ($E_x$) in the x-direction to a semiconductor sample, the carriers will travel with drift velocity ($v_d=\mu E_x$) because of the electric field ($F_e=qE_x$). At the same time, if a magnetic field ($B_z$) in the z-direction is also applied to the sample (figure1.1.1), a magnetic force ($F_m$) acts on the carriers. The electromagnetic force is orthogonal to the plane of $V_x$ and $B_z$ and causes the carriers to build up at the upper edge. The resulting charge distribution sets up an electric field called Hall field ($E_H$). The combined electric and magnetic force is given by

$$\overline{F} = e\overline{E} + e(\overline{v} \times \overline{B}) \qquad 1.1.1$$

In equation 1.1.1, $\overline{F}$ is called the Lorentz force, and deflects electrons in a direction orthogonal to both the electric current and magnetic field vectors, and the Hall field ($E_H$) arises as depicted in figure 1.1.1.

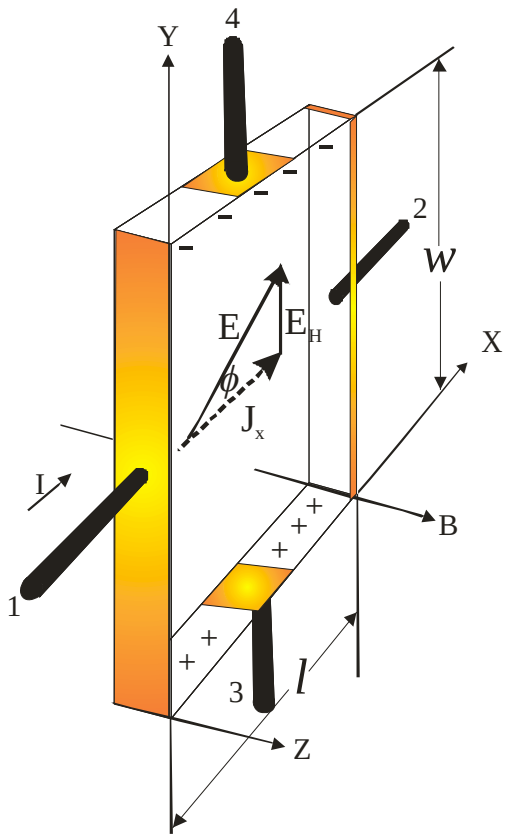



**Figure 1.1.1** Schematic shows a Hall effect in rectangular plate. Magnetic field B is along the z-axis; current density $J_x$ and Hall voltage ($E_H$) are along x- and y-axes respectively.

Electron mobility $\mu$, is given by $-e\frac{\overline{v}}{\overline{F}}$. The components of the velocity vector $\overline{v}$ in the steady state are

$$v_x = \mu(E_x - v_y B)$$

$$v_y = \mu(E_y + v_x B) \qquad 1.1.2$$

$$v_z = \mu E_z = 0$$

Under certain conditions there is no Hall voltage. This condition can be approximated by a short plate ($l<<w$) sandwiched between two large face current contacts (labelled 1 and 2 in figure 1.1.1) and the distance between them ($l$) is very short, Hall voltage is disappeared. This can be explained by using an electrical circuit. Hall voltage does not set up because the magnetic electromotive force is short-circuited by the large contacts and instead a transverse current flows. Hall effect in such a short sample is sometimes called the current deflection.[19] From equation 1.1.2 the longitudinal current density equation is

$$J_x = nev_x = \sigma\left(\frac{E_x - \mu B E_y}{1+\mu^2 B^2}\right) \qquad 1.1.3$$

where $\sigma = nq\mu$ and is the conductivity of the material. When there is no Hall voltage in sample ($E_y$=0), we consider only in x-direction, which the magnetoresistance effect is occurred. The magnetic field-dependent resistivity is $\rho(B) = \rho(0)(1+\mu^2 B^2)$. The corresponding relative increase in the material resistivity is given by

$$\frac{\rho(B) - \rho(0)}{\rho(0)} = \mu^2 B^2 \qquad 1.1.4$$

The increase in resistivity under the influence of a magnetic field due to the current deflection in a short plate is called the geometric magnetoresistance effect. It has a quadratic dependence on *B* as shown in equation 1.1.4.

### 1.1.2 Magnetoresistivity Tensor

The relation between the current density *J* and the electric field *E* is given by Ohm's law $J = \sigma E$. In the absence of a magnetic field, the conductivity $\sigma$ of an isotropic material is a scalar quantity. In the presence of a magnetic field, carriers are deflected and current density is no longer parallel to the electric field. The conductivity becomes a tensor and should be replaced by the more general expression

$$J_i = \sum_j \sigma_{ij}(B) E_j \qquad 1.1.5$$

where $\sigma_{ij}(i, j = x, y)$ are the components of the magnetoconductivity tensor $\sigma(B)$. In terms of resistivity, this relationship may be written

$$\begin{pmatrix} E_x \\ E_y \end{pmatrix} = \begin{pmatrix} \rho_{xx}(B) & \rho_{xy}(B) \\ \rho_{yx}(B) & \rho_{yy}(B) \end{pmatrix} \begin{pmatrix} J_x \\ J_y \end{pmatrix}$$

The diagonal elements $\rho_{xx}(B)$ of the magnetoresistivity tensor are measured by the ratio between the longitudinal electric field $E_x$, and the current density $J_x$.

## 1.2 The shape of semiconductors and electrodes used in Hall devices.

Any piece of electrical material, fitted with four conductive contacts, could be used as either a Hall or magnetoresistance device. However, for a device to be reasonably efficient and convenient for practical applications, it should be made in the form of a plate. In the following paragraphs, we review three main shapes of Hall and magnetoresistance sensors. These are: (i) the rectangular geometry, (ii) the Corbino disk, and (iii) the van der Pauw geometry.

- **Rectangular geometry**

The rectangular shaped plate is the most commonly used for Hall effect experiments. A short plate means the length $l$ is much smaller than the width $w$ ($l << w$). An example of a short plate was shown in figure 1.1.1.

In order to understand the influence of shape on the magnetoresistance, we will describe the magnetoresistance effect in a wide plate, as depicted in figure 1.2.1. The concentration of electrons in metals is greater by orders of magnitude than in semiconductors. The Hall angle in the metallic electrodes may thus be disregarded. These electrodes are therefore considered as equipotential surfaces.

The resistivity of the material is always measured with the electric field parallel to the current direction. The plate in figure 1.2.1 attached with large conducting area (yellow area) and use them as a current contacts.

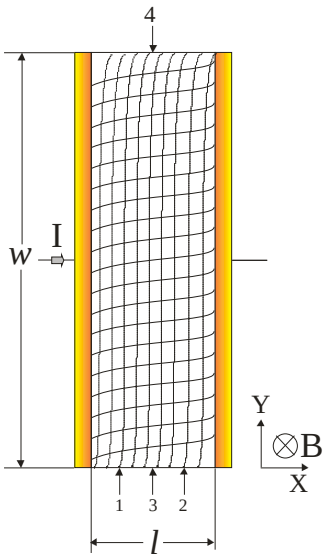



**Figure 1.2.1** Lorentz deflection in a wide semiconductor plate ($l << w$). Current lines connect contacts and are rotated from the horizontal direction by the Hall angle. Equipotential lines and lines of current flow denoted by dash and solid lines respectively; magnetic field perpendicular to the plane of the diagram (adapted from ref[20]).

If the length between the contacts is very small, the Hall voltage (measured between points 3 and 4) does not appear because the magnetic electromotive force is short-circuited by the current contacts, as discussed earlier.[19] This causes a decrease of the Hall voltage. The deflection of charge carriers from the x-direction means that the current lines between the contacts are longer, and this causes an increase in the resistance. This increase in resistance (i.e. magnetoresistance) increases with decreasing electrode distance (as short a path as it can be) and reaches its highest value in a circular disc, where the current path moves in a spiral direction from the centre to the circumference.

- **Corbino disc**

A disc structure can be prepared with one current electrode at the centre and the other around the circumference, so that current flows in a radially out direction. Magnetic field is applied perpendicular to the plane of the disc (see figure 1.2.2). Then Hall field cannot be set up and the magnetoresistance effect will be greater. This geometry is known as the Corbino disc, after Corbino who studied galvanomagnetic effect in a bismuth disc.

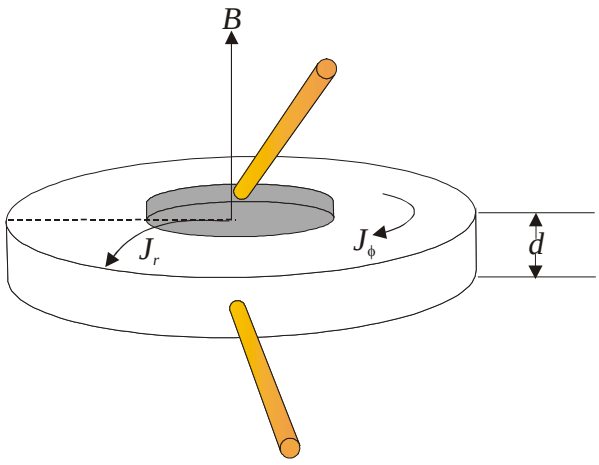



**Figure.1.2.2** Cylindrical semiconductor Corbino disc with electrodes at the centre and circumference, radial current density $J_r$, circumferential Hall current $J_\Phi$, and transverse magnetic field *B*.

The disc is the simplest geometric form that fulfils the desired boundary conditions for maximum magnetoresistance. Sometimes it may happen that the Hall coefficient is required for a specimen of arbitrary shape. Therefore if four connections are made at points along circumference, the current can passed between two of them and Hall voltage can be measured between the other two. Simultaneously, neighbouring contacts can measure the magnetoresistance effect.

This can be taken a stage further by the van der Pauw geometry.

- **van der Pauw geometry**

The van der Pauw (vdP) geometry is widely used in the semiconductor industry to determine the resistivity,[21-26] carrier concentration and Hall mobility[27-30] of uniform samples. It is also commonly used as part of experiments in crystal growth technology for either magnetic or non-magnetic material.[31-35] This geometry was originally devised by van der Pauw in 1958 so that the Hall and magnetoresistance effects could be measured on a flat sample of arbitrary shape. The advantages of this method include low cost and simplicity: the van der Pauw technique can be used on any thin sample of material. The 4 contacts are placed at the periphery of the flat sample, subject to certain conditions:

- The contacts are small relative to inter-contact distances
- The sample material is homogeneous and uniform in thickness
- The sample is thin relative to the other dimensions

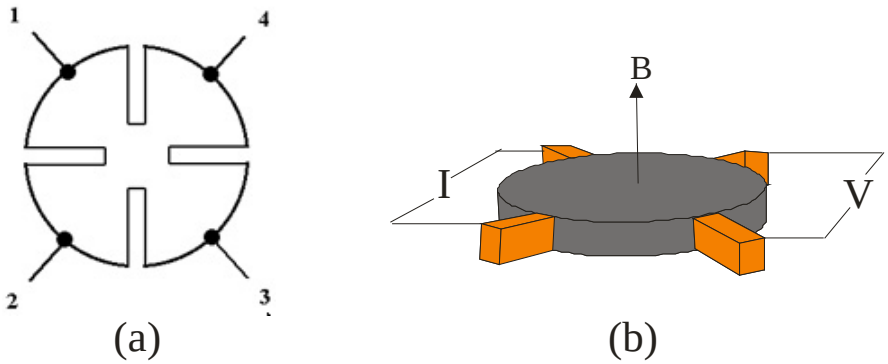



**Figure. 1.2.3** The van der Pauw (vdP) geometry (a) a clover-leaf shape (b) a circular shape: contacts are at the edge or inside the perimeter.

The apparent resistivity is obtained by passing a current through contacts 1 and 4 and determining the voltage between contacts 2 and 3 in vdP sample as shown in figure 1.2.3.

## 1.3 Extraordinary magnetoresistance

Devices based on novel magnetoresistance effects have captured the attention of many scientists. Extraordinary Magnetoresistance (EMR) is a large geometrical MR effect observed in semiconductors. The effect is dependent on physical (material parameters) and geometrical shape and electrode configuration. A typical EMR sample[16,36-39]is composed of a gold cylinder of radius $r_a$ embedded in a semiconductor ring built from a van der Pauw disc of radius $r_b$. The voltage and current probe configurations are paired as in the ordinary van der Pauw technique for the measurement of magnetoresistance.

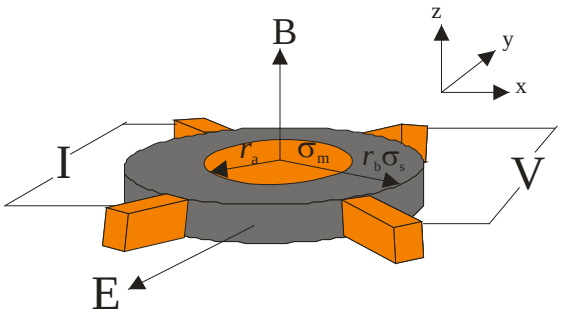



**Figure. 1.3.1** A schematic diagram of a conducting cylinder of conductivity $\sigma_m$ and mobility $\mu_m$ embedded in a semiconductor with conductivity $\sigma_s$ and mobility $\mu_s$ (after ref[38]).

Using the argument by Solin et al.[37,40] the geometrical magnetoresistance is due to the transition of the gold cylinder from a short circuit at low-magnetic fields to an open circuit at high-magnetic fields. This causes the enhancements of the magnetoresistance effect in the semiconductor even if the resistivity itself is field-independent. To explain the achievement of high values of geometrical magnetoresistance, consider the composite van der Pauw geometry as shown in figure 1.3.1, with the x-, y- and z-axes as indicated. Current flows along the x direction and a magnetic field is applied along the z direction. The magnetoconductivity tensor $\bar{\sigma}(B)$ can be expressed as:

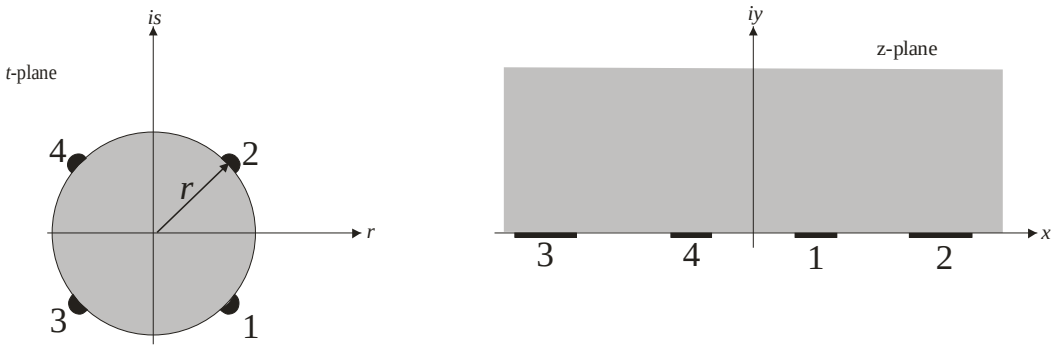
$$\bar{\sigma}(B) = \begin{pmatrix} \frac{\sigma}{1+\beta^2} & \frac{\sigma\beta}{1+\beta^2} & 0 \\ \frac{-\sigma\beta}{1+\beta^2} & \frac{\sigma}{1+\beta^2} & 0 \\ 0 & 0 & \sigma \end{pmatrix}$$

where σ is the zero-field conductivity of the semiconductor and $\beta = \mu B$. The electric field E in the sample is $E = E_x\hat{x} + E_y\hat{y}$ and the current density is given by equation (1.1.5). To conclude by Solin et al.[37,40]: 'At zero magnetic field, the magnetoconductivity tensor is diagonal and $J = \sigma E$. Thus $J // E$ and the current flows into the conducting inhomogeneity which acts as a ***short circuit***. In this case the resistance of the semiconductor slab measured along the x direction would be less than that of a homogeneous sample of the same dimensions. At high magnetic field $(\beta > 1)$, the off-diagonal of $\underline{\sigma(H)}$ $[\bar{\sigma}(B)]$ dominate and $J = \sigma/\beta[E_y\hat{x} - E_x\hat{y}]$. Then $J \perp E$ or equivalently, the Hall angle between the

electric field and the current density approaches 90°. Since the electric field is normal to the interface of the conducting inhomogeneity, this implies that the current is compelled to flow around the inhomogeneity. This deflection is total at sufficiently high fields so that the current flows only through the matrix in which case the conducting inhomogeneity acts as an ***open circuit***'. This idea will form the basis of the work presented in the first part of this thesis.

## 1.4 Bilinear Transformation

The Hall voltages for Hall plates of various shapes have been calculated using conformal mapping techniques[41-45] and finite element methods.[46-47] These methods are very convenient for developing an intuitive understanding of the influence of geometry on the characteristics of either rectangular or circular plates.




(a) (b)

(b)

**Figure 1.4.1** These two Hall plates are galvanomagnetically equivalent. (a) A circular Hall plate. (b) The corresponding half-plane Hall plate in which the current and voltage contacts are interchangeable (The illustration was adapted from the book by Popovic).[19]

The book by Popovic[19] and the papers by Zhou et al.[17] provide a succinct summary of the bilinear transformation which gives a conformal mapping between circular and rectangular plates:

Using the sequence of arguments from ref[17&19]: A device (figure 1.4.1) in the shape of a unit-radius circle in the complex *t*-plane with orthogonal axes *r* and *is* where $t=r+is$ is mapped on to the upper half-plane of a complex *z*-plane with orthogonal $z=x+iy$ by using the mapping transformation equation:

$$z(t) = -i\frac{t+i}{t-i} \qquad 1.4.1$$

Equation 1.4.1 transforms the symmetrically spaced electrical contacts on the perimeter of the disk in the *t*-plane to the corresponding contacts on the line $y=0$ in the *z*-plane. The part of the z-plane where $y>y_1$ as illustrated on the right of figure 1.4.2(a), maps to an off-centred hole ($N_1$) of radius $r_1$ in the *t*-plane, given by

$$r_1 = 1/(y_1 + 1)$$

This off-centre circle is shown on the left of figure 1.4.2(a). Consider the circles $N_2$ of radius $r_2$ in the *t*-plane as shown in figure 1.4.2(b). These circles map to a lines, which truncates the *z*-plane at the position $x=x_2=1/r_2$.

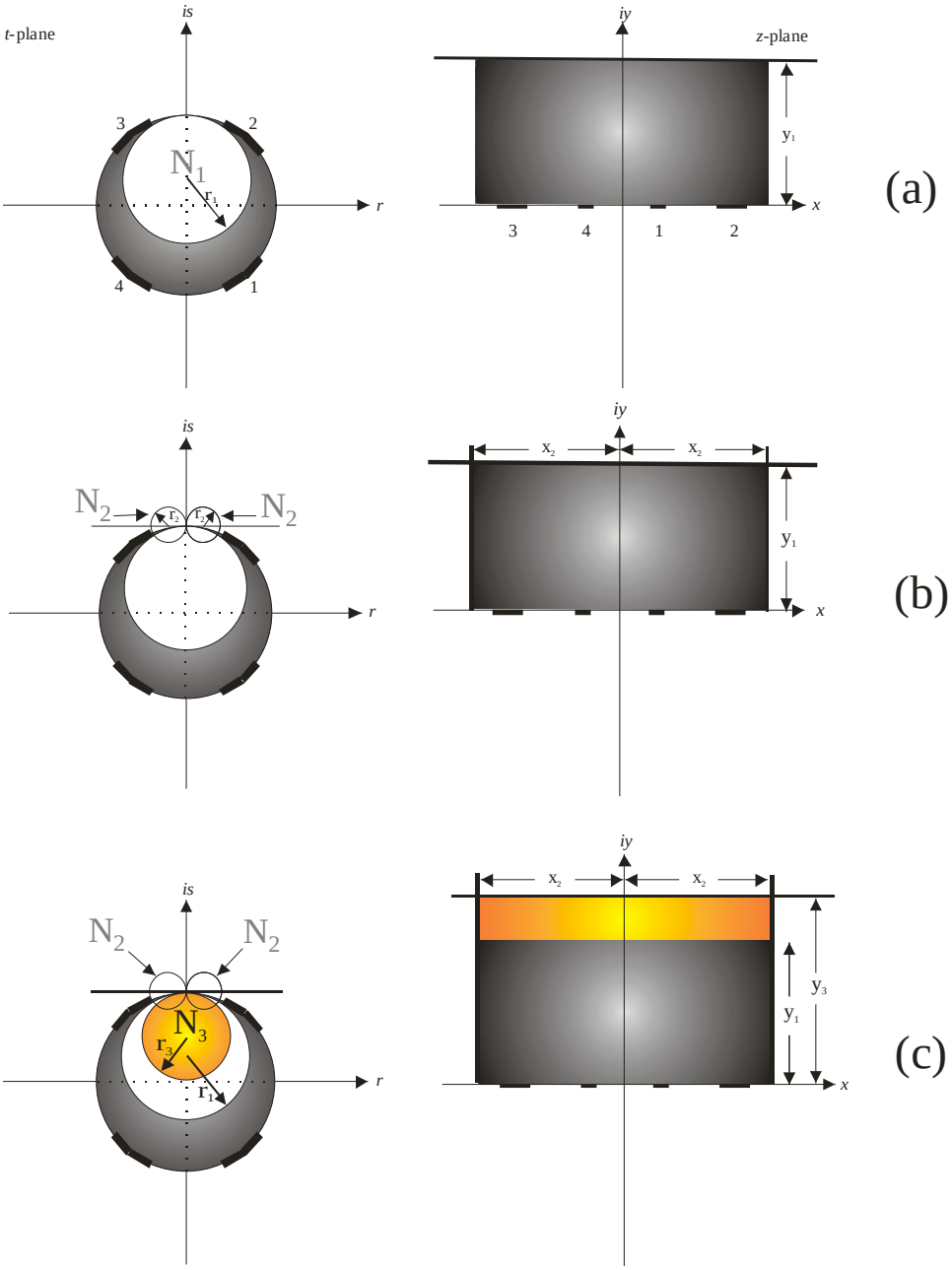



**Figure.1.4.2** Schematic diagrams of bilinear mapping of a disk in the *t*-plane mapped onto the upper half space of the *z*-plane. Also shown are the contact configurations (a) The symmetrical Hall plate on the right, which is equivalent to the disk on the left. On the disk, an off centered hole in the *t*-plane is mapped to the line $y>y_1$ in the *z*-plane. (b) The rectangular Hall plate in (a), after cutting off the portion $x > x_2$ on both sides. (c) an internal metallic circle in the *t*-plane mapped to an external metallic area in the rectangular plate (After ref [17]).

To achieve the composite vdP geometry in the form of a rectangular plate, the circle $N_3$ of radius $r_3$ adds into the *t*-plane as shown in figure 1.4.2(c). The circle $N_3$ maps to the line $y=y_3$ in the *z*-plane and placing this circle with a high conducting, the vdP geometry with an internal metallic circle $N_3$ in the *t*-plane, map to a rectangular shape in the *z*-plane with a corresponding external metallic area.

## 1.5 Review of current EMR structure and materials

There have been several new geometrical magnetoresistance (MR) sensors developed recently. It is generally agreed that materials like InSb and InAs exhibit large MR effects due to their high mobility. In 2000, Solin et al. from the NEC Princeton laboratory[37] reported very large geometrical MR enhancement when a homogeneous semiconductor (Te-doped InSb) was lithographically patterned with a cylindrical metallic inhomogeneity.

They fabricated a macroscopic composite vdP structure from a 1.3μm epitaxial InSb on GaAs with a carrier concentration $n=5.54\times10^{16}cm^{-3}$ and electron mobility of $2.9m^2/Vs$ at room temperature. The composite structure was a homogeneous semiconductor with radius, $r_b$ (=1mm), which was deposited with a metal circle of radius $r_a$. Enhancements in MR were examined by varying the ratio of $\frac{r_a}{r_b}$ (=α) for values of α=0, $\frac{1}{8}$, $\frac{1}{4}$ and $\frac{1}{2}$.

The sample inhomogeneity gave rise to MR enhancement through a transition from a short circuit at low field (B=0) to an open circuit at high field (μB>1), as was shown in section 1.3. In the four samples prepared by Solin et al.[36]

an increase in MR effect was observed with increasing α. For α=0.5, an enhancement of ~7% was observed at room temperature and B=0.05T.

The same group[38] fabricated another composite vdP structure from an epilayer of Te-doped n-type InSb with a carrier concentration $n=2.6\times10^{16}cm^{-3}$ and electron mobility $4.55m^2/Vs$ in a 1.3μm thick active layer. The parameter α (also called the filling factor) was varied from 0 to $\frac{15}{16}$. They first showed that the zero field resistance R(α,0) decreases with increasing α due to increasing conductance of the metallic inclusion. MR increased with increasing α until $\alpha=\frac{12}{16}$ or $\frac{13}{16}$, beyond which it rapidly decreased. They reported MR enhanced by 113% for $\alpha=\frac{12}{16}$ at B=0.05T and by 9,100% for $\alpha=\frac{13}{16}$ at B=0.25T and by 750,000% at 4T.

As the vdP structure is difficult to fabricate in mesoscopic sizes, to make use of the MR effect they suggested that the structure would have to be transformed into one that would be easier to fabricate. Mesoscopic size would enable measurement of small-scale magnetic domains, such as those used in magnetic recording media.

Using a bilinear transformation, Zhou et al.[17] subsequently showed that it was possible to map the composite vdP geometry onto an externally shunted rectangular plate where all contacts were at the bottom of the plate. In the same paper they reported fabricating from a Te-doped n-type InSb epilayer grown on GaAs wafer of macrosopic size (~1mm). They showed comparisons of theoretical and experimental results and achieved an EMR effect of 550% at 0.05T at room temperature. This result was obtained with a symmetrical probe configuration

(equidistant on either side of the centreline). They also experimented with asymmetric probe configuration i.e. offset from the centreline. If the placement of the voltage electrodes is asymmetric, the minimum value of the effective resistance was offset from B=0.

They proved that the rectangular EMR geometry and composite vdP were electrically equivalent. Furthermore, they showed the dependence of EMR upon the location of the current and voltage contacts. However, for a high-density recording sensor, the EMR structure must be mesoscopic in size. In 2002 Solin et al[48] reported the fabrication of a mesoscopic EMR device of dimension 200nm long, 30nm wide, 100nm deep. However, magnetotransport measurements for this device could not be made. A sample with a longer mesa (3μm) and of equivalent widths and depths was prepared. The probe configuration of this sample was asymmetrical and yielded higher EMR values than those reported in ref [17]. This EMR device was fabricated from a thin film InSb quantum well structure. The active layer was a 20nm InSb well, supplied with electrons from the 16nm thick Si δ-doped $Al_{0.09}In_{0.91}Sb$ layer, with a net donor density of $2.75\times10^{15}m^{-2}$ and a mobility of $2.3m^2/Vs$ at room temperature. The total thickness of the active layers (the supplying layers and Q-well) of this sample was approximately 0.1μm, which thus is thinner than a conventional GMR read-head (0.5-1μm). This is a significant advantage of the EMR structure as it can be placed closer to the medium.

In the same paper Solin et al. attemped to assess the impact of contact resistance on the performance of EMR devices. I-V measurements were made which showed that Au/InSb contacts were Ohmic, the EMR values measured from

this sample suggest that the room temperature performance of the device was not affected by contact resistance.

A theoretical study of the magnetoresistive response of a semiconductor bar with a T-shaped metallic shunt was reported by J. Moussa et al.[49] Calculations showed that this sample would yield MR values approximately a factor of 2.5 higher than a shuntless semiconductor bar for both IVVI and VIVI geometries.

As enhancement of mobility is important to achieve larger EMR effect Solin et al. had suggested an alternative material such as InAs with a charge mobility of $3.0 m^2/Vs$ at room temperature. Moller et al.[50] fabricated devices with a 4 nm InAs well grown by molecular beam epitaxy (MBE). The heterostructure semiconductor was patterned into a microstructured mesa with five contacts and a length of 200μm. The cleaved-edge overgrowth (CEO) technique was used to fabricate the semiconductor/metal interface with a low specific contact resistance of $10^{-8}\Omega cm^2$. The 2DES heterostructure had a carrier density of $2.85\times10^{11} cm^{-2}$ and mobility of $6.2 m^2/Vs$ at 4.2K. Illumination of the sample with 'a short pulse LED' increased the carrier density to $5.7\times10^{11} cm^{-2}$ and mobility to $14.9 m^2/Vs$. Initial investigations of EMR effect were studied for different widths (W) of semiconductor, which were 7, 20 and 70μm. They reported that the hybrid structure with the smallest width (7μm) exhibited the highest EMR of 115,000% at 4K for an unilluminated device.

Moller et al. also made extensive studies of the transfer function ($\frac{\partial R}{\partial B}$), in both the symmetric and asymmetric configurations for the lowest and highest carrier densities. The higher carrier concentrations lead to smaller values of the

transfer function. They also reported that the smaller width would obtain the higher $\frac{\partial R}{\partial B}$.

In asymmetric configurations they found asymmetric MR behaviour: $R_{min}$ was offset from B=0T. The largest value of the offset (ΔB), calculated from the difference between the minima for B+ and B- was 0.250T and 0.650T at 4.2K and 300K respectively. They obtained $\frac{\partial R}{\partial B}$=220Ω/T at B=0 in the device with W=20μm.

In their semiconductor/metal hybrid structure Moller et al.[51] assumed that the total resistance ($R_{tot}$) mainly consists of semiconductor resistance ($R_{sc}$), Au resistance ($R_{Au}$) and interface resistance ($R_i$). The Au resistance was neglected, as it is very low. They studied three different specific interface resistance ($\rho_i$) values of $1.6\times10^{-8}\Omega cm^2$, $7\times10^{-8}\Omega cm^2$ and $11\times10^{-8}\Omega cm^2$. They investigated the zero field resistance $R_{B=0}$ and the transfer function. For their device with low $\rho_i$, the $R_{B=0}$ decreased with decreasing width W of the semiconductor because the $R_{B=0}$ was dominated by the geometrical parameter. In the structure with high $\rho_i$, the $R_{B=0}$ increased with decreasing W, i.e., $R_{B=0}$ was no longer determined by the geometry alone, and the specific interface resistance dominated.

They found that a lower specific interface resistance and a smaller width both enhanced the value of $\frac{\partial R}{\partial B}$. Their smallest device was of dimension W=1.9μm and L=20μm with $\rho_i$=$7\times10^{-8}\Omega cm^2$, and exhibited a maximum $\frac{\partial R}{\partial B}$=710Ω/T. The EMR effect of this device was 1290% at 1T and 4.2K.

## 1.6 Geometry of the samples

In the case of the rectangular plate, the magnetoresistance is diminished because the Hall field acts to reduce the Lorentz force. In contrast, the Corbino geometry does not support a space charge. At $B=0$ the current flows radially between the concentric electrodes. At finite magnetic field $B$, the Lorentz force causes the current trajectories to be spirals. This results in an increase of the effective length of the current path, leading to increase MR effect. Unfortunately, the Corbino geometry cannot be modified to the exact desired shape and wired up with an inner electrode. The composite van der Pauw structure differs from rectangular plate and Corbino disc. This geometry shows how such geometrical effect can be exploited to enhance the magnetoresistance effect.

By transforming the composite vdP into the rectangular structure all contacts are positioned at one side of the plate. In this thesis we study magnetoresistance (MR) of homogeneous semiconductors in rectangular structures equivalent to the composite vdP geometry that contain different metallic patterns, and observe the MR effect enhancement in each pattern. The rectangular structure yields an MR effect equivalent to that in the Extraordinary Magnetoresistance (EMR) structure, introduced by Solin et al.[48-53] The structure of all the samples in this thesis is based on the rectangular form with six leads as electrodes along one edge, as illustrated in Figure. 1.5.1.

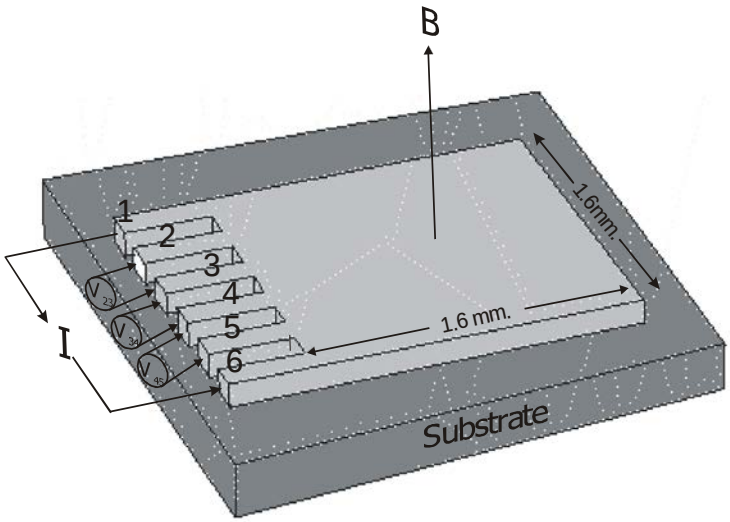



**Figure 1.5.1** The structure of the devices. The contacts labelled 1 and 6 are used as current contacts, while contacts 2, 3, 4 and 5 are used as voltage probes.

In order to measure the magnetoresistance of structure, a current is passed between the source (lead 1) and drain contacts (lead 6) and the leads in between are used to measure voltages. The MR effect of the metal-semiconductor structure is described by

$$EMR(B) = \frac{R(B)}{R_{\min}} - 1 \ (\%)$$

expressed as a percentage, where *R(B)* is the resistance in a field *B* and $R_{\min}$ is the minimum resistance. These are defined by

$$R(B) = \frac{V(B)}{I}$$

$$R_{\min} = \frac{V_{\min}}{I}$$

We can exploit the properties of the structure by using it in either symmetric or asymmetric probe configurations, as will be described in chapter 3.

## 1.7 GaSb/InAs/GaSb Hetrostructures

Hall devices and magnetoresistors have become increasingly important in both microelectronics and sensor applications in the last decade. Currently, III-V compounds such as InAs and InSb are the favoured materials. As relative changes in resistance are proportional to the square of charge mobility, and InSb has the highest mobility of any semiconductor at room temperature, this material has been used for magnetoresistors. However, the band-gap energy of InSb is small (0.17 eV). While Si has a larger bandgap but a rather low mobility, an alternative choice such as InAs is attractive because the energy gap of InAs is larger than InSb and the mobility is higher than GaAs (as high as InSb), as listed in Table 1.

Recently, with the development of epitaxial growth techniques, it is now possible to fabricate high quality III-V heterostructures. The use of a III-V two-dimensional electron gas (2DEG) seems to be an effective method for producing a high electron mobility and a low sheet electron density.

**Table 1** Some parameters of materials

| Material | Bandgap (eV) | | Carrier concentration ($cm^{-3}$) | Electron mobility at 300K ($cm^2/Vs$) |
|---|---|---|---|---|
| | 300K | 0K | | |
| Si | 1.12 | 1.17 | $1\times10^{10}$ | 1,500 |
| InSb | 0.17 | 0.23 | $2\times10^{16}$ | 80,000 |
| InAs | 0.36 | 0.42 | $1\times10^{15}$ | 33,000 |
| InAs/GaSb 2DEG | | | $n_s=2.7\times10^{12}\,cm^{-2}$ | 24,000 |

The devices in the first part of this study use a high-mobility two-dimensional electron system (2DES) in a semiconductor heterostructure. The system used in the study is the lattice-matched combination InAs/GaSb.

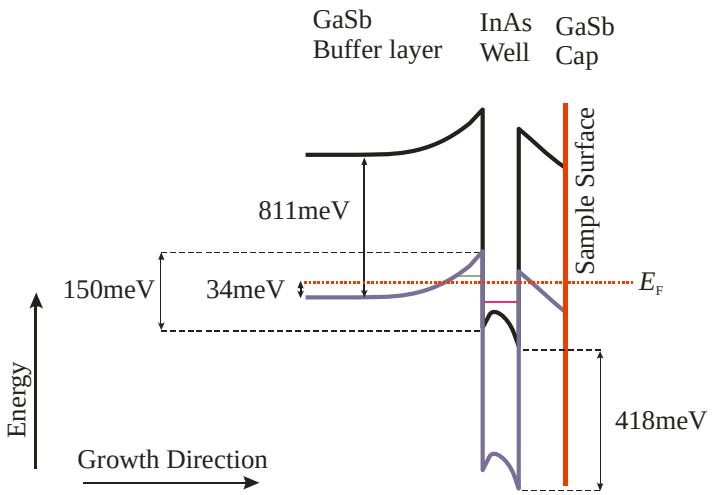



**Figure. 1.6.1** The band line-up of an GaSb/InAs/GaSb heterostructure.

InAs and GaSb are group III/V semiconductors and crystallize with the usual zinc blende structure. Both have direct band gaps at the gamma point in k-space. The GaSb/InAs/GaSb heterostructure is known as a broken gap in which the GaSb valence band lies approximately 150 meV above the conduction band of InAs. A schematic diagram of the band structure of a GaSb/InAs/GaSb heterostructure is illustrated in Figure 1.6.1. When the two materials are brought together at interfaces, the band gap overlap induces charge transfer from the GaSb valence band to the InAs conduction band to equalize the Fermi level across the structure.

## 1.8 References


[1] J. Heremans, D. L. Partin, C.M Thrush, L.Green, *Semicond. Sci. Technol*. 8 (1993) S424-S430.

[2] Y. Sugiyama, *J. Vac. Sci. Technol*. B13(3) (1995) 1075-1083

[3] O.Yilmazoglu, M. Brandt, J. Sigmund, E. Genc, H.L. Hartnagel, *Sensors and Actuators* A94 (2001) 59-63

[4] I. Shibasaki, *Journal of Crystal Growth* 175/176 (1997) 13-21.

[5] A. Lapicki, H. Sanbonsugi, T. Yamamura, N. Matsushita, M. Abe, H. Narimatsu, H. Handa, A. Sandhu. *IEEE Trans. Mag*. 41(10)(2005) 4134-4136

[6] A. Sandhu, H. Handa, *IEEE Trans. Mag*. 41(10)(2005) 4123-4127

[7] J. Kvitkovic, M. Majoros, *J.Magnetism&Mag.Mat* 157/158(1996) 440-441

[8] S A Solin, R A Stradling, T Thio and J W Bennett, *Meas. Sci. Technol.* 8 (1997) 1174-1181

[9] S.S.P. Parkin, *Appl. Phys. Lett*. 69 (20), (1996).

[10] S. Foss-schroeder, J. Van Ek, D. Song, D. Louder, G. Al-jumaily, P. Ryan, C. Prater, E. Hachfeld, M. Wilson, and R. Tench. *J. Appl. Phys.* Vol. 89(11), 6769 (2001).

[11] W. Ricken, J. Lui and W.J. Becker. *Sensors and Actuator* A91 (2001) 42-45.

[12] W. Vartsch, G. Rupp and W. schelter. *Sensors and Actuator* A46-47 (1995) 302-306.

[13] W.F. Egelhoff, *J. Appl. Phys*. 78, 273 (1995).

[14] L. Romashev, A Rinkevich, A. Yuvchenko, A. Burkhanov, *Sensors and Actuator* A91(2001) 30-33

[15] P. Ripka, *Sensors and Actuator* A41-42(1994) 394-33

[16] T.Thio and S.A. Solin**,** *Appl. Phys. Lett*. 72, 3497(1998).

[17] Zhou,-T.; Hines,-D.-R.; Solin,-S.-A., *Appl Phys Lett*. 29 Jan. 2001; 78(5): 667-9.

[18] R.A. Stradling in: *III-V Quantum Wells and Superlattices*, Eds. P. Bhattacharya, Inspec, Exeter (1996), p.375.

[19] R.S. Popovic, *Hall Effect Devices* (Hilger, Bristol, 1991)

[20] S.M.Sze in: Semiconductor sensors, Wiley-Interscience Publication, p215.

[21] Weishart,-H.; Heera,-V.; Eichhorn,-F.; Pecz,-B.; Barna,-A.; Skorupa,-W., *Journal-of-Applied-Physics*. 15 July 2003; 94(2): 1195-204.

[22] Rietveld,-G.; Koijmans,-Ch.-V.; Henderson,-L.-C.-A.; Hall,-M.-J.; Harmon,-S.; Warnecke,-P.; Schumacher,-B., *IEEE-Transactions-on-Instrumentation-and Measurement*. April 2003; 52(2): 449-53.

[23] Lenssen,-D.; Carius,-R.; Mantl,-S.; Birdwell,-A.-G., *Journal-of-Applied-Physics*. 1 Oct. 2001; 90(7): 3347-52.

[24] Shayegan,-M.; Manoharan,-H.-C.; Papadakis,-S.-J.; Poortere,-E.-P.-D., *Physica-E*. Feb. 2000; 6(1-4): 40-2.

[25] Koon,-D.-W.; Castner,-T.-G., *Physical-Review-B-Condensed-Matter*. 15 June 1990; 41(17): 12054-70.

[26] Levy,-M.; Sarachik,-M.-P., *Review-of-Scientific-Instruments*. July 1989; 60(7) pt. 1: 1342-3.

[27] Gerhard,-A.; Harneit,-W.; Brehme,-S.; Bauknecht,-A.; Fiedeler,-U.; Lux-Steiner,-M.-C.; Siebentritt,-S., *Thin-Solid-Films*. 29 May 2001; 387(1-2): 67-70.

[28] K. Makoto, T. Mishima, *Journal of Crystal Growth* 175/176 (1997) 844-848

[29] Pfeifer,-L.; West,-K.-W.; Stormer,-H.-L.; Baldwin,-K.-W., *Applied-Physics-Letters*. 30 Oct. 1989; 55(18): 1888-90.

[30] Patel,-D.; Crumbaker,-T.-E.; Sites,-J.-R.; Spain,-I.-L., *Review-of-Scientific-Instruments*. Nov. 1986; 57(11): 2795-7.

[31] Eisener,-B.; Wagner,-M.; Wolf,-D.; Muller,-G., *Journal-of-Crystal-Growth*. March 1999; 198-199 pt. 1: 321-4.

[32] Foxon,-C.-T.; Cheng,-T.-S.; Jeffs,-N.-J.; Dewsnip,-J.; Flannery,-L.; Orton,-J.-W.; Harrison,-I.; Novikov,-S.-V.; Ber,-B.-Ya.; Kudriavtsev,-Yu.-A., *Journal-of-Crystal-Growth*. June 1998; 189-190: 516-18.

[33] P.R. Hageman, V. kirilyuk, W.H.M. Corbeek, J.L. Weyher, B. Lucznik, M. Bockowski, S. Porowski, S. Muller, *Journal-of-Crystal-Growth*. 255(2003) 241-249

[34] J. Mimkes, V. Sestakova, K.M. Nassr, M. Lubbers, B. Stepanek, *Journal-of-Crystal-Growth*. 187(1998) 355-362

[35] M. Thomas, H.R. Blank, K.C. Wong, K. Kroemer, *Journal-of-Crystal-Growth* 175/176 (1997) 894-897

[36] Zhou,-T.; Solin,-S.-A.; Hines,-D.-R., *Journal-of-Magnetism-and-Magnetic-Materials*. May 2001; 226-230 pt. 2: 1976-7.

[37] Solin,-S.-A.; Hines, T.Thio, *Physica B* 279(2000) 37-40.

[38] S.A. Solin, T.Thio T.Thio, D.R. Hines, and J.J. Heremans, *Science* 289, 1530(2000).

[39] J. Moussa, L.R. Ram-Mohan, J. Sullivan, T. Zhou, D.R. Hines, and S.A. Solin, *Phys. Rev. B* 64, 184410(2001).

[40] S.A. Solin, T.Thio T.Thio, D.R. Hines, M Kawano, N. Oda and M. Sano, *Journal-of-Applied-Physics* 85, (1999) 5789-5791

[41] Wick R.F., *J. Appl. Phys*, 25, 741-56 (1954)

[42] D. S. Perloff, Solid-State. Electron. 20 (1977) 681-687

[43] D. S. Perloff, Solid-State. Electron. 21 (1978) 1013-1018

[44] Kuhrt F and Lippmann H. J, *Hallgenerator* (Berlin: Springer) pp 72-82 (1968)

[45] Versnel W, *Solid-State Electron*. 24 63-8 (1981)

[46] I.S. Ibrahim, V.A. Schweigert and F.M. Peeters, *Physical Rev B.57*, no.24, 15416(1998).

[47] Y.G.Cornelissens and F.M. Peeters, *J. Appl. Phys*. 92, (2002) 2006-12.

[48] S.A. Solin, D.R. Hines, J. S. Tsai, Y. A. Pashkin, S. J. Chung, N. Goel, and M. B. Santos, *IEEE Trans. Magn*. 38, 89(2002).

[49] J. Moussa, L.R. Ram-Mohan, A.C.H. Rowe, and S.A. Solin, *J. Appl. Phys*. 94, 1110(2003).

[50] C.H. Moller, O. Kronenwerth, D. Grundler, W. Hansen, C. Heyn, and D. Heitmann, *Appl. Phys. Lett*. 80, 3988(2002).

[51] C. H Moller.; Grundler,-D.; Kronenwerth,-O.; Heyn,-C.; Heitmann,-D., *Journal-of-Superconductivity*. Feb. 2003; 16(1): 195-9.

[52] S.A. Solin, D.R. Hines, A. C. H. Rowe, J. S. Tsai, Y. A. Pashkin, S. J. Chung, N. Goel,

and M. B. Santos, *Appl. Phys. Lett*. 80, 4012(2002).

[53] Solin,-S.-A.; Hines,-D.-R.; Rowe,-A.-C.-H.; Tsai,-J.-S.; Pashkin,-Y.-A., *Journal-of-Vacuum-Science-&-Technology-B-Microelectronics-and-Nanometer-Structures*. Nov. 2003; 21(6): 3002-6.

# Chapter 2

# Experimental Techniques and Device Fabrication

2.1. Introduction……..……..31

2.2. Growth Techniques……..……..31

2.3. Device Fabrication……..……...32

2.4. Measurement…… 35

*2.4.1 The calibration of the vdP Hall sensors.……..……36*

*2.4.2 Electrical and Magnetotransport Measurement.……...…..…37*

2.5. References……..……..…41

# 2. Experimental Techniques and Device Fabrication.

## 2.1 Introduction

This chapter presents the experimental methods employed on GaSb/InAs/GaSb double heterostructures. The experiments concern transport measurement at temperatures of 4.2K, 77K and 300K. Measurements have made by using continuously varying magnetic fields from $-0.3<B<0.3$T for 77K and 300K while a superconducting magnet was used at 4.2K. Some basic properties of the material will be described.

Firstly before transport measurement can be made wafer must be processed into a device. This involves etching a mesa of the appropriate shape and depositing a metallic pattern and ohmic contacts on to the sample. The fabrication of the sample structures is also described.

## 2.2 Growth Techniques

The samples studied in this thesis were grown by metal-organic vapor phase epitaxy (MOVPE) by P. Shield, N.Mason and P.Walker.[1-2] Growth occurs at atmospheric pressure, with a heated substrate sitting parallel to a laminar flow. In MOVPE, hydrogen is used as the carrier gas with metal-organic precursors for the group III elements and an organic compound for the group V elements. A chemical reaction occurs at the heated surface substrate and then epitaxial layers of group III and V atoms are deposited on substrate. The surface photoabsorption

(SPA) technique[3,4] is used to monitor the growth of different layers. The growth rate in MOVPE can be up to ten times faster than Molecular Beam Epitaxy (MBE). Hence MOVPE is often the growth system of choice in large-scale production of commercial devices due to its lower cost. All samples discussed in chapter 3 and 4 come from MOVPE growths on quarter wafer pieces of three-inch GaAs substrates.

A 2 μm thick buffer layer of GaSb is first grown on the substrate. This is followed by the InAs well of 25 nm, and a GaSb Cap of 80 nm. The grown layers are cleaved into smaller pieces for device processing. Photolithography is employed to deposit appropriate patterns on the semiconductor surface.[5-7] This procedure must be carried out in a clean room to avoid contamination so the suite of class 10,000 clean rooms within the Physics Department were used to process all the devices.

## 2.3 Device Fabrication

Photolithography involves the patterning of a semiconductor surface using a photoactive material called photoresist[8] in our case is a positive one. The optical masks were prepared by printing out a large-scale picture of the patterns and then reducing to the actual size and optically transforming them onto glass plates. The sequence is summarized schematically in Figure 2.3.1.

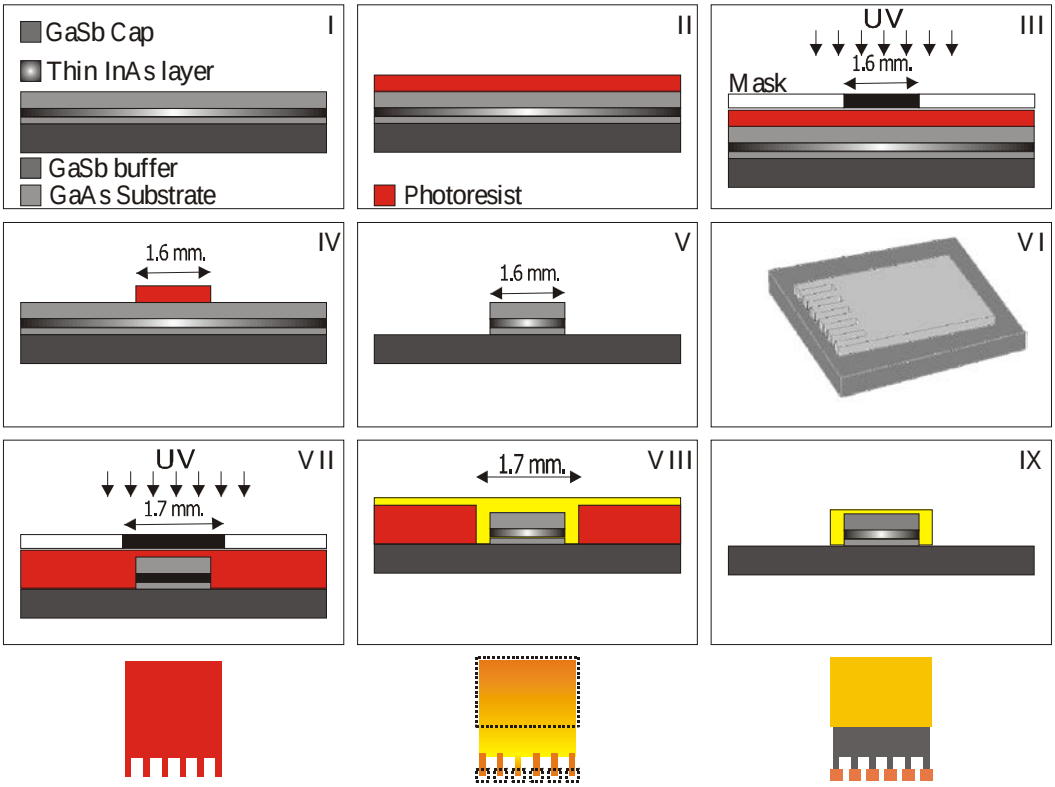



**Figure 2.3.1** Sample fabrication schematic.

I. ***Cleaning and degreasing sample***. The sample must be kept very clean throughout the fabrication process. Grease or dust particles, which could prevent the adhesion of the photoresist or metallization to the surface, must be removed. The sample is first immersed in 1,1,1 – trichloroethylene, a good solvent for grease. The sample is then cleaned in acetone and isopropanol to remove any surface residues and then dried by blowing it with nitrogen. The samples are put on a hotplate at 100 °C for 1 minute to drive off any solvent or water; this dehydration baking promotes a better adhesion of the photoresist.

II. ***Spinning photoresist layer***. A photoresist is spun onto the surface while the sample mounted on a spinner vacuum chuck. I have used Shipley

S1813 photoresist, which gives a layer 1.3 μm thick when spun at 4000 rpm for 45 seconds. The sample is then pre-baked on the hotplate at 90 °C for 1 minute to evaporate the majority of the solvent from the resist layer.

III. ***Aligning and exposing***. The mask is interposed between the UV light source and the coated wafer. The sample is brought into contact with the pattern side of the mask and then positioned so that the pattern will be defined on the appropriate region of the sample. Regions of photoresist layer, not masked by the pattern are then exposed to a 200-Watt UV lamp for 16 seconds.

IV. ***Developing***. The sample is then removed from the mask aligner and placed in the microposit MF319 developer for 60 seconds and rinsed thoroughly with de-ionised (DI) water. The exposed resist dissolves in the developer leaving the area that was protected by the mask. One can check the layer has been fully developed by viewing the sample with a microscope using a yellow filter in front of the light source. The sample may then be developed further if necessary.

V. ***Etching.*** The photoresist pattern is then used as a mask for etching. The samples are dipped in HCl for a few seconds to remove oxides of GaSb, and then put in a mixture of $C_6H_8O_7$:$H_2O_2$:$H_2O$, in the ratio of 2:1:1 by volume. The etching properties of this mixture have been characterized by J. Rehman[9] who found almost vertical etch profiles. The etch rate was up to 0.4μm per minute.

VI. ***Removing photoresist***. The photoresist etched mask is then dissolve in acetone, which removes both exposed and unexposed photoresist.

VII. ***Contacts and Pattern Alignment***. The next stage is to spin a photoresist for contacts mask. The first four steps of the procedure are repeated using a different mask with metallic and contact patterns. To avoid mismatching the contact mask with the mesa mask, I designed the length of the contact mask longer than the mesa mask so that it overlaps on both sides.

VIII. ***Ohmic contacts and Evaporation***. The samples are then mounted in a metal evaporator, and the chamber is pumped to a vacuum of about $1\times10^{-6}$ mbar. For ohmic contacts, a 140 nm layer of Au/Ge followed by 100 nm of gold is evaporated onto the GaSb surface of the sample so that the metal layer goes over the mesa edge. The samples are then annealed at 400 °C for 10 seconds in a saturated $N_2/H_2$ atmosphere. At this temperature the metals partly diffuse into the semiconductor forming ohmic contacts to the active layers (InAs).

IX. ***Lift off.*** The sample is immersed in acetone. This process dissolves the photoresist under the metallization film and also lifts-off the evaporated metal except for the regions where the contacts and patterns were defined. The contacts are then bonded using a Gold Ball Bonder. The size of the ball is 100μm.

## 2.4 Measurements

Two stages of measurements were performed in this study. The first stage involved the calibration of the vdP Hall sensor that we used to measure the real-time magnetic field from the magnetic coil. The second stage involved a

magneto-transport measurement of the samples.

### 2.4.1. The calibration of the vdP Hall sensor

A small electromagnet was used to produce the magnetic field for the experiments at room temperature and 77K. The coil was powered from a Thurlby Thandar Instruments PL330DP, thus generating a magnetic field between $-0.3<B<0.3$T. The vdP sensor is encapsulated in epoxy resin to protect the surface and is attached to one of the poles. We calibrated the sensor using a hand held Hall probe, Hirst GM04 gauss meter with accuracy of better than ±1%. A constant current of 1mA is driven through vdP sensor, the Hall voltages are measured with a Keithley 196 DVM while the gauss meter simultaneously measured the magnetic field from the coil.

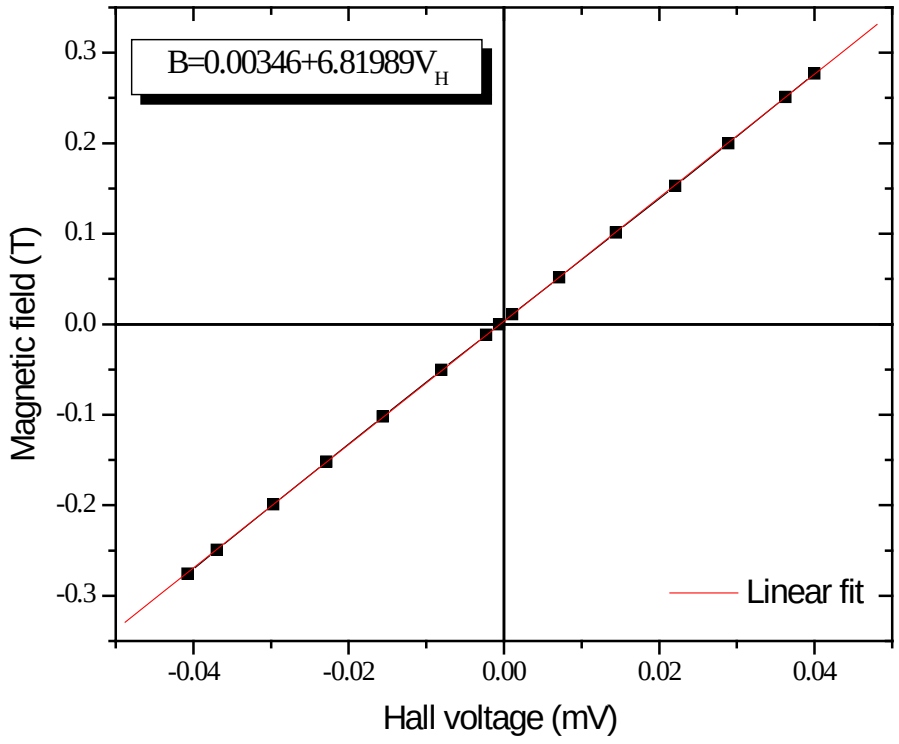



**Figure2.4.1** The linear curve fit for a magnetic field reading.

The Hall voltages and the reading magnetic field are plotted as shown in figure 2.4.1. The sensor has a Halll voltage varies linearly with the magnetic fields; a linear equation is shown in an inset. Therefore when we measure the output voltage from the vdP sensor, we can then convert the output voltage into a field reading.

### 2.4.2 Electrical and Magnetotransport Measurement

After the processing steps described in section 2.3 the sample is protected by packing so that it can be handled easily.

- **Room temperature and 77K**

The magneto-transport measurements were carried out using a standard AC lock-in technique. An AC voltage from a lock-in amplifier was driven through a series resistor to give a current of 1mA. The current is fed via the source and the drain contacts of the sample. A schematic illustration of this circuit is shown in Figure 2.4.2.

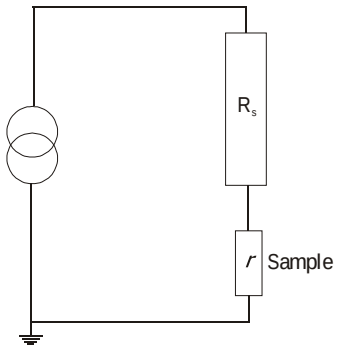



**Figure 2.4.2** A simplified test circuit of a sample with a series resistance ($R_s$).

The voltages across the sample measured by the lock-in amplifier. The input impedence of the lock-in was 100 MΩ and always much greater than the resistance of the sample.

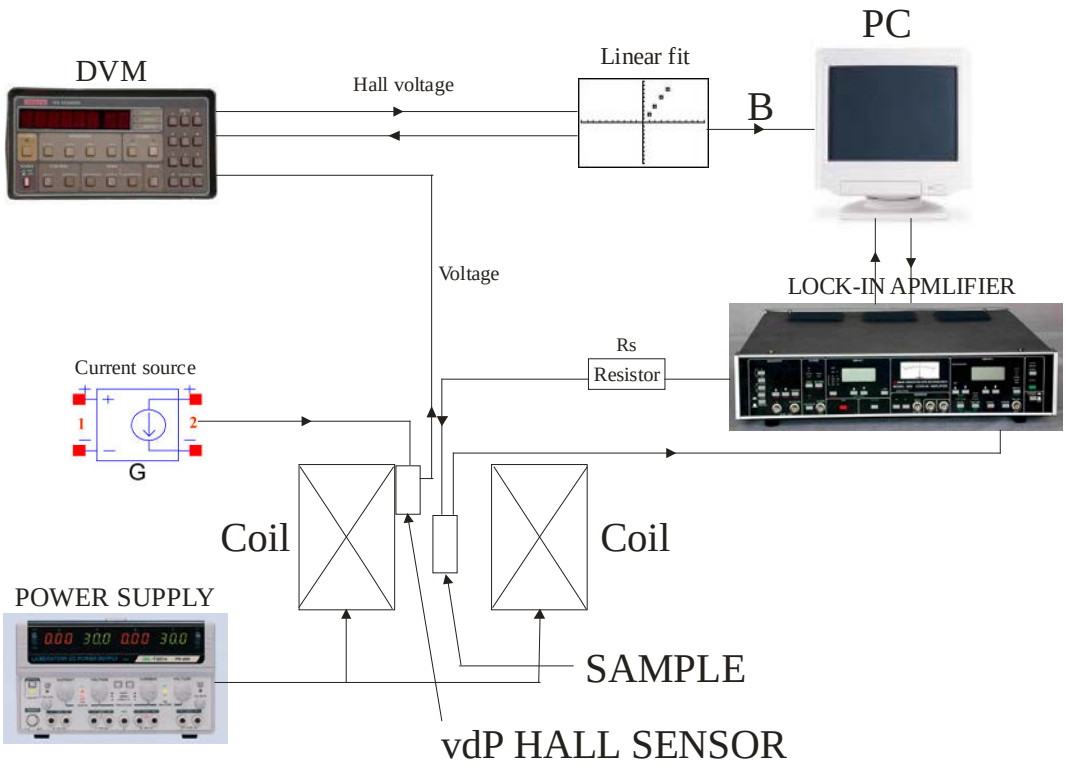



**Figure. 2.4.3** Transport measurement set-up.

A labview program written by T.Stadlemann carries out initialization procedures, controls the power supply to the magnet coils, acquires the current and voltage data through an IEEE-488 interface card. It converts output voltages of the vdP sensor to magnetic fields, and plots the B-V trace. The equipments set-up is shown in figure 2.4.3.

For measurement at 77K, we used the same set-up apparatus as at room temperature, but a vessel of liquid nitrogen were used to cool the samples down. The samples were mounted on an insert and then immersed into the liquid nitrogen. The sample and the vessel are then placed between the magnetic poles. The level of liquid nitrogen was carefully controlled throughout the experiment to

ensure that the measurement was carried out at exactly 77K.

- **Low temperature measurements (4.2K)**

The low temperature measurements described in this part were performed using the Oxford Instruments superconducting magnet capable of producing fields up to 17 T at 4.2K. The magnet consists of two nested selonoids immersed in a bath of liquid helium. The inner coil is made from multifilament $Nb_3Sn$ and the outer coil is NbTi. The magnetic field inside the 50 mm bore is calibrated to 0.01% accuracy and is homogeneous to 0.1% within 1 cm of the field center. The magnet power supply operates at a maximum output of 120A and 10V.

Samples were mounted on an insert, then placed inside a stainless steel tube, and cooled to 77K with liquid nitrogen. It was then lowered slowly into the magnet cryostat until the samples are in the center of the field.

## 2.5 References


[1] G.R. Booker, P.C. Klipstein, M. Lakrimi, S. Lyapin, N.J. Mason, R.J. Nicholas, T-Y. Seong, D.M. Symons, T.A. Vaughan, P.J. Walker, *J. Cryst. Growth*, 145, 778(1994).

[2] G.R. Booker, M. Daly, P.C. Klipstein, M. Lakrimi, R.F. Kuech, S. Lyapin, N.J. Mason, I.J. Murgatroyd, J. C. Portal, R.J. Nicholas, P.Vicente, D.M. Symons, P.J. Walker, *J. Cryst.Growth*, 170, 77(1997).

[3] D.A. Allwood, N.J. Mason, P.J. Walker, *J. Cryst. Growth*, 163(1998).

[4] D.A. Allwood, N.J. Mason, P.J. Walker, *J. Cryst. Growth*, 168(1998).

[5] M.C. King, *VLSI Electronics*, Vol. 1. Eds. N.G. Einspruch, Academic, New York, (1981).

[6] J.H. Bruning, *Semiconductor Technology*, *Electrochemical* Soc, Eds. D.A.Doane, D.B. Fraser, D.W. Hess, Penningston, (1982).

[7] R. Williams, *Modern GaAs processing methods*, Artech House, Boston, (1990).

[8] W.S. Deforest, *Photoresist Materials and Processes*, Mcgraw-Hill, New York, (1975)

[9] Y.J. Rehman, *D.Phil. Thesis*, oxford (1996).

# Chapter 4

# The Influence of geometry and Conclusions

4.1 The extraordinary magnetoresistance and the sensitivities of samples……95

4.2 Devices applications ……...……..…99

4.3 References……...…….…..103

# 4 The Influence of geometry and Conclusions

Geometrical effects as described in the previous chapter have shown a result in a large enhancement of the magnetoresistance effect. Examples of material that exhibit this effect are narrow-gap semiconductors, zero-gap mercury cadmium telluride ($Hg_{1-x}Cd_xTe$)[1-3] and two-dimensional electron gases (DEG).[4] Our studies have extended the geometrical magnetoresistance effect to new hybrid metal-semiconductor geometries. The large magnetoresistance can be seen as resulting from current deflection by the metal inhomogeneity.

In this chapter, first of all, we present the sensitivities of sample $M^E05$. Secondly we chose R14 for type I, $M^E05$ for type II and T10 for type III, which give the highest EMR effect as shown in chapter 3 to show the EMR values and the sensitivities. In the final section, we show the tip metallic pattern as a potential candidate for read-head sensor when it is fabricated in a smaller dimension.

## 4.1 The extraordinary magnetoresistance and the sensitivities of samples

The development of the extraordinary magnetic sensor has focused on high sensitivity and high resolution. Although researchers in the field try to increase MR ratios, as measured in the 4 contacts configuration a more useful criterion for sensor applications is often the absolute sensitivity or the change in resistance per magnetic field. To enable a comparison to be made with other magnetic sensors, it is useful to characterize magnetoresistance sensors in a similar way to Hall devices, which also operate in a 4 contacts configuration.

In this section we first show the magnetoresistance values and the sensitivities of sample $M^E05$, which is the semiconductor mesa with the triangular metallic pattern as described in chapter 3. Sample $M^E05$ showed the largest relative magnetoresistance, $\frac{R(B_{max})}{R_{min}}$, when measure with a symmetric probe configuration. The field dependence of the room temperature resistances for both configurations, the symmetric ($R_{34}$) and the asymmetric ($R_{23}$, $R_{45}$) configurations are shown in figure 4.1.1.

The minimum resistance of $R_{23}$, $R_{34}$ and $R_{45}$ are about 18.2, 4.26 and 3.04Ω respectively. At B = –0.275T, the resistances $R_{23}$, $R_{34}$ and $R_{45}$ increase to values of 43.44, 20.71 and 8.91Ω respectively. Therefore the corresponding magnetoresistances are 238%, 486% and 293%. The central probes ($R_{34}$) give the highest value for the EMR effect.

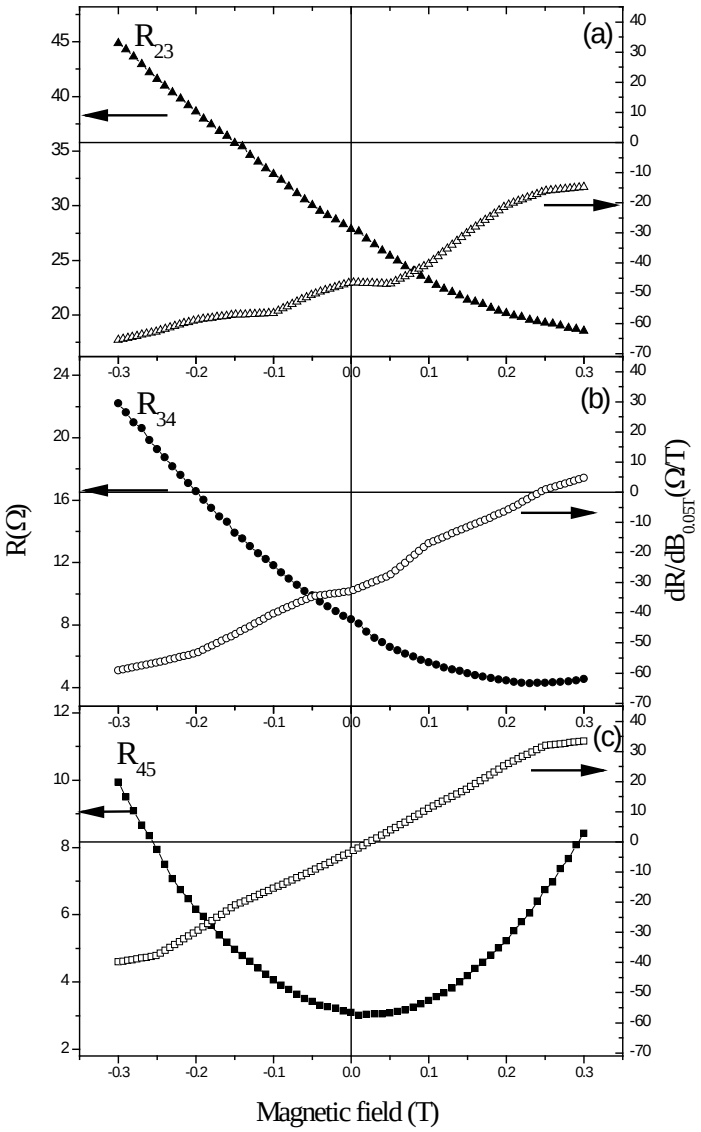



**Figure 4.1.1** Magnetoresistances of the sample $M^E05$ at room temperature. (a) and (c) represent the data set of the asymmetric configurations $R_{23}$, $R_{45}$ respectively. (b) represents the symmetric configuration. The filled symbols denote the magnetoresistance values and the opened symbols denote the sensitivities $\frac{d(R)}{d(B)}$.

The derivative of *R(B)* gives the absolute sensitivity $\frac{d(R)}{d(B)}$ as also shown in figure 4.1.1. The derivative is taken by averaging the slopes of two adjacent data points as follows:

$$\frac{1}{2}\left(\frac{R_{i+1}-R_i}{B_{i+1}-B_i}+\frac{R_i-R_{i-1}}{B_i-B_{i-1}}\right)$$

At room temperature sensitivities of –46.3, -32.8 and –3.35Ω/T are found at $B$=0 for $R_{23}$, $R_{34}$ and $R_{45}$ respectively. From the EMR using relative resistivity values showed that the sample $M^E05$ has maximum EMR of 486% for the $R_{34}$ contact configuration. In contrast, the maximum absolute sensitivity of 46.3Ω/T is found for the $R_{23}$ configuration.

Secondly, we chose the largest EMR effects from the three main patterns to compare the EMR values and the sensitivities of the samples using different criteria. The pattern chosen are R14, $M^E05$ and T10 for type I, II and III respectively.

The three different criteria that we use are

- The change in relative resistance $\frac{R(B_{\max})}{R_{\min}}$ which is a commonly used criterion in the previous literature.
- $\frac{R(B=0.05T)}{R_0}$ which measures the relative resistivity change brought by a field of 0.05T. This is the typical value of field that would be available in applications such as read-heads for magnetic disks.
- $\frac{dR(0)}{d(B)}$ which is the absolute resistivity change, and which is directly comparable to values which could be measured using Hall effect sensors.

**Table 4-1** The EMR values and the sensitivities of three main patterns at ±0.275T. All probe configurations measured at room temperature.

| Sample | $R(B_{max})/R_{min}$ | | | | | $R(B=0.05T)/R_0$ | | | | | $dR(0)/d(B)$ | | | | |
|---|---|---|---|---|---|---|---|---|---|---|---|---|---|---|---|
| | $R_{23}$ | | $R_{34}$ | $R_{45}$ | | $R_{23}$ | | $R_{34}$ | $R_{45}$ | | $R_{23}$ | | $R_{34}$ | $R_{45}$ | |
| R14 | 5.03 | | 3 | 5.99 | | 1.25 | | 1.05 | 1.19 | | 23.7 | | -1.8 | -30.1 | |
| $M^E05$ | 2.38 | | 4.86 | 2.93 | | 1.08 | | 1.2 | 1.1 | | -46.3 | | -33 | -3.4 | |
| T10 | $R_{23}$ | $R_{34}$ | $R_{35}$ | $R_{45}$ | $R_{56}$ | $R_{23}$ | $R_{34}$ | $R_{35}$ | $R_{45}$ | $R_{56}$ | $R_{23}$ | $R_{34}$ | $R_{35}$ | $R_{45}$ | $R_{56}$ |
| | 3.66 | 7.79 | 2.31 | 8.99 | 3.64 | 1.14 | 1.27 | 1.05 | 1.28 | 1.14 | 50.2 | 11.3 | -2.6 | -12 | -54 |

It can be seen that optimum performance based on all three indicators is achieved using the metallic tip pattern. For the optimised performance of samples as the EMR sensors, we would use the sample T10 of metallic tip pattern (type III) combines with inner probe configuration ($R_{34}$, $R_{45}$) as they show the highest EMR. While the best sensitivity obtain from the sample T10 combine with outer probe ($R_{23}$, $R_{56}$) configuration.

## 4.2 Device applications

In general, the magnetoresistance sensors may be considers as magnetic transducer; they translate the input magnetic induction into a corresponding electrical output signal. Recently, It has been suggested by the several groups of scientist to employ the EMR effect in metal-semiconductor hybrid structure for creating high-density magnetic recording applications.[5-9] A mesoscopic nonmagnetic magnetoresistive read-head sensor has been fabricated.[5] The observed EMR at the relevant field of 0.05 T is 4.75 %; the value field chosen is the field that the sensor can access for a given read-head design with modern disk

media. This sensor has a conservatively estimated potential to enable data storage with a real density of 10 Gb/in$^2$.

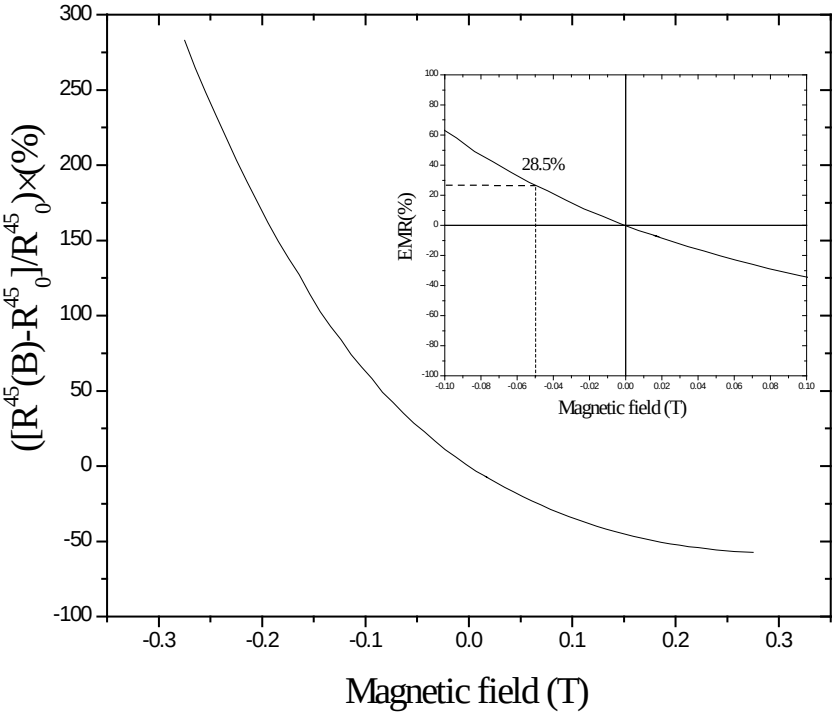



**Figure 4.2.1** The room temperature EMR of the metallic tip pattern as described in chapter 3. Sample T10 measured with inner probe configuration ($R_{45}$). Inset shows the EMR at the relevant field of 0.05T is 28.5 %.

For our macroscopic devices (1.6mm×1.6mm), the metallic tip pattern has been chosen as they shown the best performance in here. The pattern is symmetric and gives the highest EMR effect when measured by the inner probe configurations ($R_{34}$, $R_{45}$). Since the magnitudes of EMR are similar, we present only $R_{45}$. The resultant EMR in a low field is shown in figure 4.2.1.

The EMR is defined as $\frac{R^{45}(B)-R_0^{45}}{R_0^{45}}$, where $R^{45}(B)$ is the resistance in a magnetic fields *B*, and $R_0^{45}$ is the resistance in zero field using the voltage probe 4 and 5. As can been seen from figure 4.2.1, the observed EMR of the tip pattern at the relevant field 0.05 T is 28.5%. Therefore the tip pattern described in this thesis could be an interest pattern for read-head applications. Simultaneously, the dimension of the sample does matter, as a density of the magnetic recording is inversely proportional to the sensor's size. Therefore this sample needs to be fabricated in a smaller dimension. The recent work of EMR device from different material and dimension are listed in table 4-2.

**Table 4-2** The summary of R14 and EMR devices reported elsewhere.

| **Parameters** | **R14** | | **InSb** | | **InAs** | |
|---|---|---|---|---|---|---|
| | | | **[ref.6]** | **[ref.7]** | **[ref.8]** | **[ref.9]** |
| **Structure** | 2DES InAs/GaSb | | Doped InSb epilayer | Q-well $InSb/In_{1-x}Al_xSb$ | 2DES InAs/InGaAs | |
| **$n/n_s$ ($cm^{-3}$/ $cm^{-2}$)** | 300K | $n_s=2.7\times10^{12}$ | $n=2.11\times10^{16}$ | $n_s=2.7\times10^{11}$ | | |
| | 4K | $n_s=9.98\times10^{11}$ | | | $n_s=2.85\times10^{11}$ | $n_s=2.85\times10^{11}$ |
| **Mobility ($m^2$/Vs)** | 300K | 2.7 | 4.02 | 2.3 | | |
| | 4K | 13.9 | | | 6.2 | 6.2 |
| **Dimension** | Macroscopic | | Macroscopic | Mesoscopic | Microscopic (200×7μm) | Microscopic (2×1.9 μm) |
| **EMR** | 300K | 25% AC B=0.05T | 550% AC B=0.05T | 35% AC B=0.05T | | |
| | 4K | 3150% SC B=0.3T | | | 115000% SC B=1 T | 1290% SC B=1T |

AC = asymmetric probes configuration

SC = symmetric probes configuration

For data storage applications, EMR has many advantages over conventional devices. Neither the semiconductor nor the metallic pattern is magnetic material; therefore the demagnetising process is not required. Moreover, The asymmetric design either from probe configurations or asymmetric metallic pattern generates a zero-field offset. It can use to distinguish the magnetic field direction.

## 4.3 References


[1] T.Thio, S.A. Solin, J.W. Bennett, D.R. Hines, M. Kawano, N. Oda, and M. Sano, *Phys. Rev. B* 57, 12239(1998).

[2] T.Thio, S.A. Solin, J.W. Bennett, D.R. Hines, M. Kawano, N. Oda, and M. Sano, *J. Cryst. Growth* 184-185, 1293(1998).

[3] S.A. Solin, T.Thio, J.W. Bennett, D.R. Hines, M. Kawano, N. Oda, and M. Sano, *Appl. Phys. Lett*. 69, 4105(1996).

[4] J. Heremans, D. L. Partin, D.T. Morelli, B. K. Fuller and C.M. Thrush, *Appl. Phys. Lett*. 57 (3), 1990, 291-293

[5] S.A. Solin, D.R. Hines, J. S. Tsai, Y. A. Pashkin, S. J. Chung, N. Goel, and M. B. Santos, *IEEE Trans. Magn*. 38, 89(2002).

[6] Zhou,-T.; Hines,-D.-R.; Solin,-S.-A., *Applied-Physics-Letters*. 29 Jan. 2001; 78(5): 667-9.

[7] Solin,-S.-A.; Hines,-D.-R.; Rowe,-A.-C.-H.; Tsai,-J.-S.; Pashkin,-Y.-A., *Journal-of-Vacuum-Science-&-Technology-B-Microelectronics-and-Nanometer-Structures*. Nov. 2003; 21(6): 3002-6.

[8] C.H. Moller, O. Kronenwerth, D. Grundler, W. Hansen, C. Heyn, and D. Heitmann, *Appl. Phys. Lett*. 80, 3988(2002).

[9] Moller,-C.-H.; Grundler,-D.; Kronenwerth,-O.; Heyn,-C.; Heitmann,-D., *Journal-of-Superconductivity*. Feb. 2003; 16(1): 195-9.

# Part II Vertical Hall Sensors

# Chapter 5

# Introduction

5.1 Introduction……..……...…105

5.2 Materials and Technology……...……106

5.3 Basic physical consideration…….…….106

*5.3.1 Hall Voltage*……...……..107

*5.3.2 Offset*……...……108

*5.3.3 Sensitivity*……...…….109

5.4 Interpretation……..110

5.5 References……..112

# Part II Vertical Hall Sensors

## 5.1 Introduction

Hall sensors are used widely in applications today. They are not used just to measure magnetic field, but also as key components in contactless sensors for linear position and angular position. Recently, many research groups and industrial companies attempt to reduce the sensor's dimensions.[1-3] By combining Hall sensors with miniaturized magnets, they are also attractive for applications of magnetic RAM.[4-5]For conventional Hall effect sensors, both current injection and measurement of the Hall voltage take place in a plane parallel to the surface of the wafer on which they are fabricated. In this geometry, the sensors are restricted to measuring the component of the magnetic field normal to the surface of the device. However, there are some applications where sensitivity to the magnetic field parallel to the device surface is preferred. In the Vertical Hall device[6-9] that can detect magnetic field parallel to the surface in which the current is flowing perpendicular to the surface and is therefore sensitive to magnetic field parallel to the wafer surface.

In this part of the thesis, we report on a study and design of in-plane sensing performance of an etched mesa, which is called the Vertical Mesa Hall Sensor (VMHS). We have fabricated these from the III-V compound semiconductor, which is an InSb wafer. This is a promising material for magnetic sensor devices, because it exhibits large electron mobility near room temperature, and could be an excellent material to fabricate highly sensitive Hall elements for practical magnetic sensor applications.

## 5.2 Material and Technology

As we have described in part I, the galvanomagnetic effect for Hall plates is governed by the mobility and magnetic field product $\mu B$. This seems to favour materials with high mobility. Thus, InSb and InAs seem to be superior to GaAs and Si.

A good Hall device is made from a material having a low carrier concentration and high carrier mobility. This criterion is best met in semiconductors. In 1948, Peason[10]proposed the instrument that was able to measure a magnetic field as exploited the Hall effect in a germanium probe. Many years later, Bosch[11] proposed that the Hall devices are compatible with the epitaxial integrated circuit. More recently, Hall sensors have been in strong demand in the field of electronic equipment in many applications.

We distinguish two groups of Hall sensors by their response to a magnetic induction vector: either perpendicular or parallel to the chip surface. In the first, the magnetic vector is perpendicular to wafer surface such as for the Hall Plate. In the second, the integrated Hall sensors respond to a magnetic induction vector parallel to the chip plane. Such an integrated Vertical Hall Device (VHD) can be manufactured in a standard IC technology.[9]

## 5.3 Basic physical Considerations

A magnetic field sensor is a device able to convert the magnetic field induction (B) into an electrical signal. The electrical characteristics of a Hall device operate in the conventional way: the device is biased via its two non-neighbouring contacts. The Hall voltage is considered as the output signal.

### 5.3.1 Hall voltage

The Hall effect is illustrated schematically in figure 5.3.1, the charge carrier experiences a force in a direction perpendicular to both the magnetic field and carrier velocity as expressed in equation 1.1.1 in chapter 1.

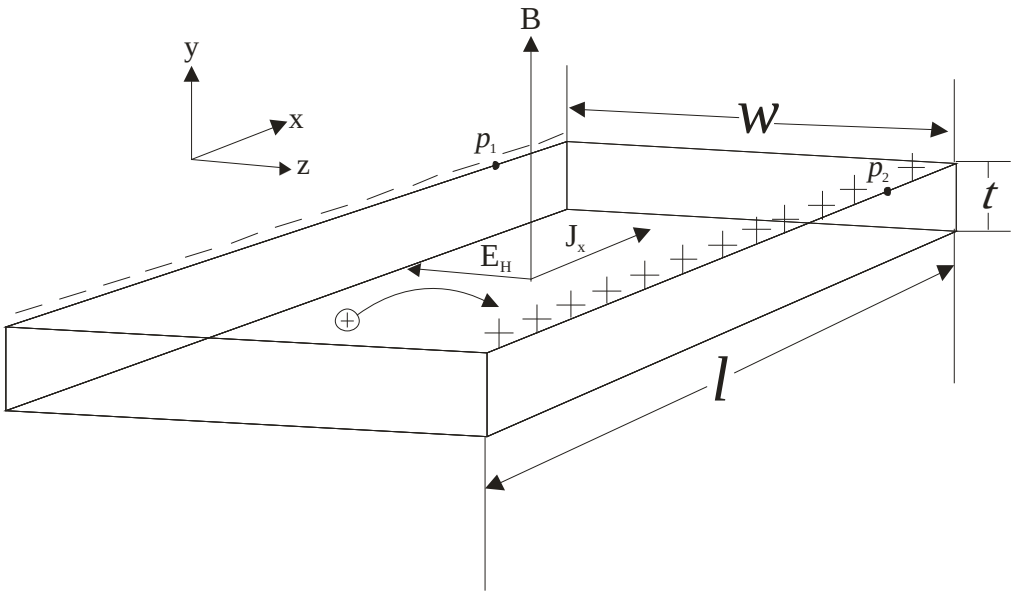



**Figure 5.3.1.** The Hall effect in a long rectangular plate (*l*>>*w*). B is the magnetic field in y-direction, $J_x$ is the current density, $E_H$ is the Hall field (z-direction). The magnetic forces push both positive and negative charge carriers towards the upper boundary of the plate. The Hall voltage appears between the charged edges of the plate.

Integrating the Hall field with respect to position across the width of the plate produces the Hall voltage $V_H$. Consider a point contact Hall plate, shown in figure 5.3.1. The Hall voltage of a point contact Hall device is given by

$$V_H = -\frac{1}{ne}\int_{p_1}^{p_2}[J \times B] \bullet dz \qquad 5.3.1$$

where $n$ is a carrier concentration. Assuming that the Hall device is a homogeneous plate of thickness $t$, and the magnetic induction is uniform over the plate, equation 5.3.1 can be rearranged with the total bias current of the device $I$ given below

$$\left|\frac{V_H}{I}\right| = \frac{1}{net} B_{\perp} \qquad 5.3.2$$

where we have neglected the minus sign, while assuming that the points $p_1$ and $p_2$ lie on the same equipotential plane. Equation 5.3.2 shows that the Hall voltage is proportional to the lower carrier concentration, and the thickness of the plate.

### 5.3.2 Offset

An offset voltage exists in a real Hall device because of the imperfections in the fabrication process such as misalignment of contacts, non-homogeneities of material, and mechanical stress[12] by the packaging process. The causes of offset voltage in Hall device can be represented using the simple bridge circuit model of a Hall plate.[13] The schematic of a bridge circuit is shown in figure 5.3.2.

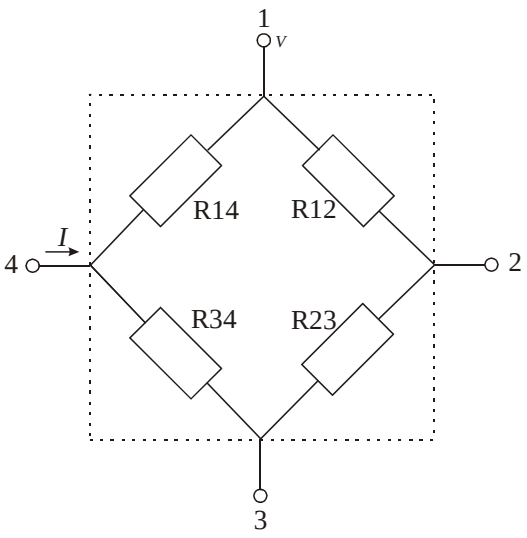



**Figure 5.3.2.** Schematic of bridge circuit with the four resistors to approximate behaviour of a Hall plate.

The imbalance of four resistors on the bridge circuit caused the offset voltage. To cancel or reduce offset voltages, a Hall plate with maximum possible symmetry is needed. There are several methods introduce for reducing the offset, such as by wiring the resistor to re-balance the resistors in the device (invented by Thomson in 1856).[14] The so-called spinning current method[15-16] is also widely used for reducing the offset voltage, but an additional circuit is required for this method.

### 5.3.3 Sensitivity

Sensitivity is the important figure of a sensor. In general, the current and the voltage sensitivity of a rectangular Hall device (figure 5.3.1) can be expressed as follows:

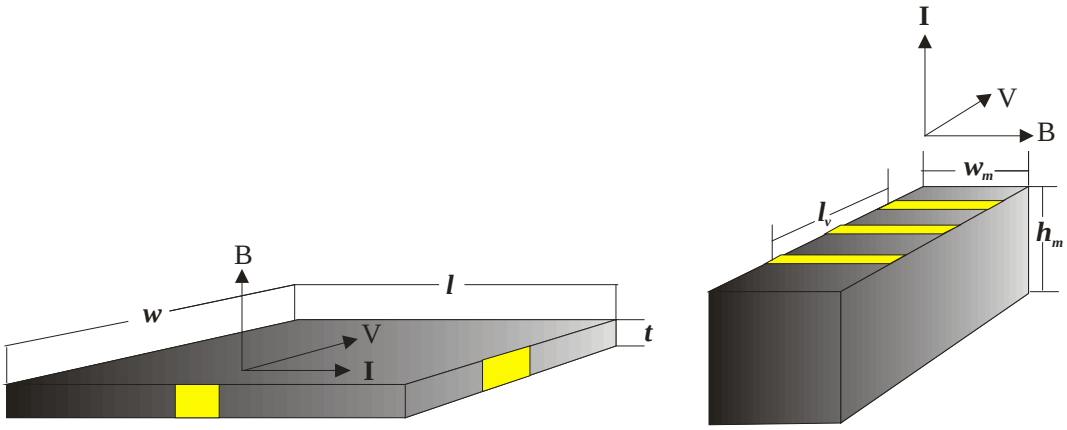
$$S_I = \frac{1}{I_D}\frac{dV_H}{dB} \cong \frac{1}{N_s e} G_H \qquad 5.3.3(a)$$

$$S_V = \frac{1}{V_D}\frac{dV_H}{dB} \cong \mu \frac{w}{l} G_H \qquad 5.3.3(b)$$

where $I_D$ and $V_D$ are the current and voltage drive respectively, $G_H$ is the geometrical correction factor, which depends on the device geometry (length-to-width ratio) and Hall angle. The geometrical correction factor is a number limited by $0< G_H <1$. As we have replaced *nt* by sheet carrier density $N_s$, the units of $S_I$ and $S_V$ are $VA^{-1}T^{-1}$ and $T^{-1}$, respectively.

## 5.4 Interpretation

A theoretical calculation of the sensitivity of VMHS generally has to take into account the precise geometry of the device. However, it is reasonable to expect that, because of the unique shape of the device, a good approximation can be obtained by considering the mesa as a simple geometry. The thickness (*t*) in the conventional geometry is determined in the direction of the magnetic field, which is perpendicular to the I-V plane, thus the thickness is equivalent to the width ($w_m$) of the mesa in VMHS. The lengths and the widths of the conventional geometry are the distances between the current and voltage contacts, respectively. Thus the lengths and the widths of the conventional geometry are equivalent to the mesa height ($h_m$) and the length ($l_v$) between voltage contacts in VMHS geometry (see in Fig. 5.3.3).




(a) (b)

**Figure 5.3.3.** (a) Conventional Hall plate geometry (b) The design of the Vertical Mesa Hall Sensor (VMHS).

The equation (5.3.3) shows that the sensitivities of the device depend on the physical and geometric parameters. In the conventional Hall plate, decreasing the thickness and carrier concentration can increase the current sensitivity; In the VMHS the thickness of the plate is equivalent to the mesa width, therefore decreasing the width gives higher current sensitivity.

The voltage sensitivity strongly depends on the mobility and the width-to-length ratio; so the higher mobility the higher voltage sensitivity is obtained.

Table 5-1 Equivalent parameters for Hall plate and Vertical Mesa Hall sensors (VMHS)

| **Parameters** | **Hall plate** | **VMHS** |
|---|---|---|
| **Thickness of the plate** | $t$ | $w_m$ |
| **The distance between current contacts** | $l$ | $h_m$ |
| **The distance between voltage contacts** | $w$ | $l_v$ |

## 5.5 References


[1] T. Kanayama, H. Hiroshima, M. Komuro, *J. Vac. Sci. tech*. B6(3) (2001) 1010

[2] Y. Sugiyama, *J. Vac. Sci. tech*. B13(3)(1995) 1075

[3] A. Sandhu, H. Masuda, A. Oral, S.J. Bending, *J. Cryst. Growth* 227-228 (2001) 899-905.

[4] Y.G. Cornelissens, F.M. Peeters, *J.Appl.Phys*. 92(4)(2002) 2006-12

[5] V. Cambel, Micro. Electro. Eng. 51-52(2000) 333-342.

[6] R. S. Popovic, *IEEE Electron Dev. Lett*. EDL-5 (9) (1984) 357-358.

[7] A. M. J. Huiser, H. P. Baltes, , *IEEE Electron Dev. Lett*. EDL-5 (11) (1984) 482-484.

[8] E. Schurig, C. Schott, P.A. Besse and R. S. Popovic, Proc. *16th Eurosensors Conference, Prague, Czech Republic*, (2002) 868-871

[9] E. Schurig, M. Demierre, C. Schott and R. S. Popovic, *Sensors & Actuators* A: 3184 pp. (2002)1-7

[10] G.L. Pearson, *Rev. Sci. Instrum*. 19 (1948) 263-5.

[11] G. Bosch, *Solid-State Electron*. 11, 712 (1968)

[12] R. Steiner, Ch. Maier, M. Mayer, S. Bellekom, H. Baltes, *J. Microelectromech. Syst***.** 8(4) (1999) 466-472.

[13] R.S. Popovic, *Hall Effect Devices* (Hilger, Bristol, 1991).

[14] Thomson W, *Philos. Trans. R.. Soc*. (1856) A146 736-751.

[15] P. J. A. Munter, *Sensors and Actuators*, A25-27 (1991) 747-751.

[16] P. J. A. Munter, *Sensors and Actuators*, A21-23 (1990) 743-756.

# Chapter 6

# Design consideration and Fabrication

6.1 Design consideration……..115

6.2 Fabrication Process…….116

6.3 Samples……..119

6.4 Measurement……..120

*6.4.1 Hall voltage*……...……121

*6.4.2 Current dependence*…….……122

*6.4.3 Angular dependence*……122

6.5 References…….…….123

# 6. Design consideration and Fabrication

Early Hall devices for magnetic sensor applications were made in the form of a plate. They are sensitive to the magnetic field where the field is normal to their surface. The efficiency of a Hall magnetic sensor, the sensitivity, is higher when the plate thickness is small, so good Hall plates have to be thin. A lateral magnetic sensor that is sensitive to a field parallel to the device surface, and can be manufactured in standard IC technology is the Vertical Hall sensor (VHS), recently devised by Popovic et. al.[1] These devices were fabricated using standard bulk CMOS technology. Another device using CMOS process is a trench-Hall device.[2] This device related to various pre-processing steps in order to force the current go deeper into the device, i e., to improve the sensitivity. However, the complicated fabrication process might cause their device having problem in reliability and stability.

Our devices, the Vertical Mesa Hall Sensor (VMHS) created by taking a conventional Hall bar design and turning it on its side. A number of modifications have to be made, to enable fabrication on an InSb wafer using conventional lithographic techniques.[3-5] The Hall bar is maintained as a separate insulated shape which is defined by etching the wafer to leave a mesa. In this design, the conducting substrate acts as one of the current contacts.

In this chapter, we describe the design considerations, the fabrication procedure followed by a description of the sample geometry used and then the measurement methods employed.

## 6.1 Design consideration

In order to achieve device which is sensitivity to magnetic induction parallel to the wafer surface, the active region of a conventional Hall device is rotated by 90° with respect to the substrate (Fig.6.1.1). For technological reasons, the positions of the contacts have to be rearranged. The lower current contact and the second set of voltage probes (not needed for a sensor) are eliminated. The contacts are moved to the top to provide the basic shape of the proposed device. Also devices requiring contact that electrically connects to the bottom of the mesa, this is placed on the substrate next to the mesa, and is called the back contact.

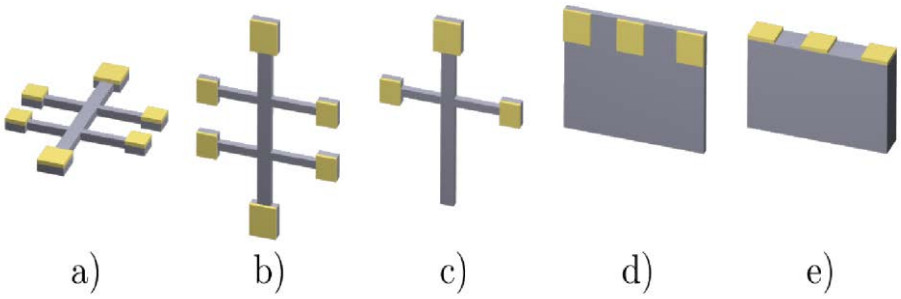



**Figure 6.1.1.** Turning a Hall bar on its side. (a) Starting from a conventional Hall Bar (b) Hall device with a vertical orientation with respect to the substrate. (c) The lower current contact and the second set of voltage probes (not need for the sensor) are eliminated. (d-e) The contacts are moved to the top to provide the basic shape of the proposed device.

The surface of the etched area and the sidewalls of the mesa are covered with a dielectric to enable the creation of insulated interconnects. The insulating layer chosen for this purpose is $SiO_2$

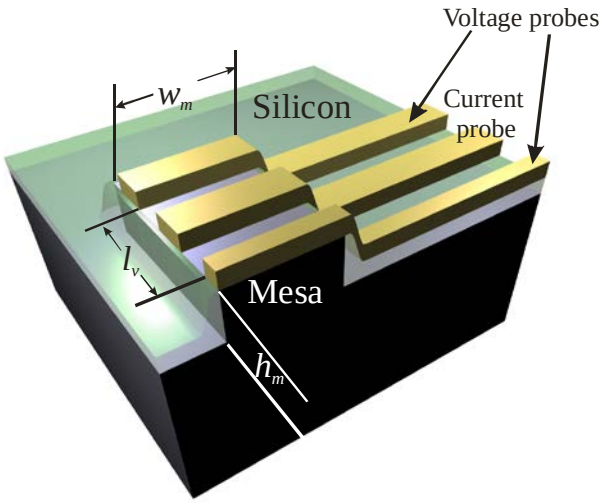



**Figure. 6.1.2.** The design of the vertical Mesa Hall Sensor (VMHS)

The principle of such a device, realized in conventional lithography is shown in Figure 6.1.2. We have created a number of devices with a range of mesa sizes, contact sizes and spacings. For ease of optical processing, we work with a minimum contact width and spacing of 2 μm (going up to 8 μm) and a corresponding mesa area of $30\times12\mu m^2$ (going up to $400\times25\mu m^2$). The height of the etched mesa is 1.5μm.

## 6.2 Fabrication Process

In order to physically define the mesas and contacts, various techniques were used. These involved wet etching to produce the mesa, then thin film techniques to coat dielectric over the etched surface as an insulating layer, and metallization to produce ohmic contacts as illustrated in figure 6.2.1. The fabrication process in Part II is similar to Part I.

An etch mask, covering the areas of the mesa and the hole for the back contact, is defined by standard photolithography techniques.

A wet etching technique was used to etch away to the intended depth without removing the etch mask. The following recipe was used for wet etching for the samples are: 0.5M $K_2Cr_2O_7$: $CH_3COOH$: 10M HBr, ratio 1:1:1 by volume. The etch-profile was measured using an atomic force microscope. When the sample stayed in the solution for 30s the mesa edge was defined as a step over 1.5μm high.

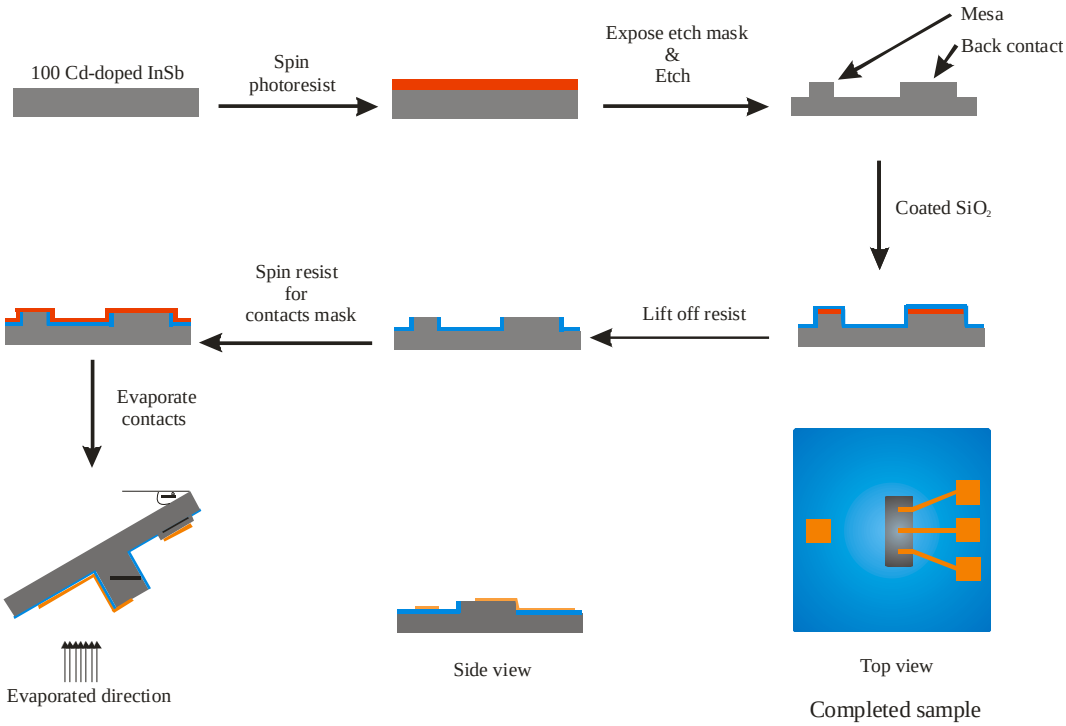


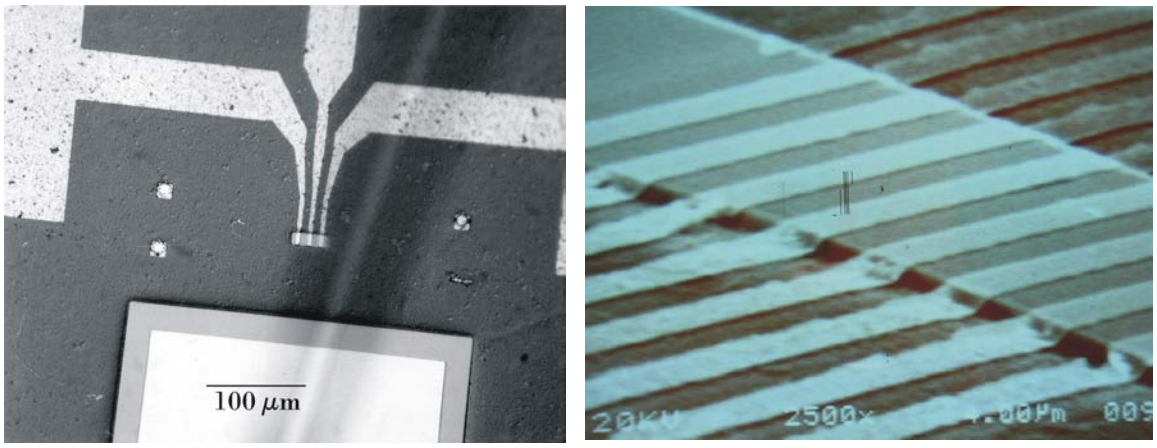

**Figure 6.2.1.** Sample preparation for VMHS using standard photolithography, then thin film for insulating layer of SiO2, and final step of making contacts.

For the insulating layer, the sample is then placed in an evaporator and covered with a 100 nm $SiO_2$ layer. In order to avoid current injection through the sidewalls of the mesa, the evaporation is performed at an angle to the normal and

the sample is rotated during the process, which ensures sufficient coverage of the sides. Evaporated $SiO_2$ tends to organise into pillar-like structures, leaving pinholes in between. These can provide an ohmic conduction path, which has initially been a problem for the successful production of working devices. In order to obtain a good insulator, it is found to be necessary to prevent this growth mode by introducing irradiation with a low-energy (≈ 100eV) oxygen ion beam into the evaporation procedure. This enables us to grow higher insulating dielectric layers with a moderate breakdown voltage of 1.0±0.2V.

After deposition of the insulating layer, the photoresist is removed. In the second lithographic step, an evaporation mask for the contacts and interconnects is defined. A gold layer with a nominal thickness of 200 nm is then evaporated on top of a thin nickel layer, which helps the sticking of the gold to the semiconductor. As the gold interconnects are frequently disconnected at the sidewalls of the mesa, we tilt the sample at the angle of 30 ° ± 5° with respect to the direction of the evaporation. Finally, the samples were diced and individual chips were bonded for testing.

The substrate is contacted through a separate window in the $SiO_2$ layer as shown in figure 6.2.2(a). The success of the angled evaporation that makes the gold contacts connected through the mesa is shown in figure 6.2.2(b).




(a) (b)

**Figure 6.2.2.** Optical pictures of VMHS. (a) A simple Vertical Mesa Hall sensor, the back contact on the substrate can be seen at the bottom. (b) An angled evaporation made the gold contacts and the SEM show that the contacts are connected to the top of mesa.

During the process, we have found that because of the angled evaporation and the small distances between the contacts, complete lift-off is difficult to achieve after deposition of the metal layer. In a large number of samples, connections between the metal contacts or interconnects prevent proper operation of the devices. We have succeeded in producing the working devices in a small amount of samples, which will show in the next section.

## 6.3 Samples

The samples were fabricated from (100) Cd-doped InSb wafers. The material is intrinsic at room temperature with an electron Hall mobility of $4.4 \times 10^4$ $cm^2/Vs$ and a carrier concentration of $3.2 \times 10^{16}$ $cm^{-3}$. The initial motivation in this part is to study the new geometry for Hall sensors so low carrier density p- or

n-type InSb can be used to produce the device provided that it has high room temperature mobility.

The samples were divided into 2 types of mesa. The first type is a short mesa, which has a mesa size of 30×12, 48×12μm$^2$ and has been etched a depth of 1.5μm. The short mesas were patterned into several contacts width 4μm and spacing of 8μm (VH-48) and another short mesa has contact width 8μm and spacing of 8μm (VH-88). The short mesa is our simplest VH structure and has 3 contacts on the mesa surface and back contact on the substrate. The second type is long mesa, which has a mesa size of 400×25μm$^2$ with 13 contacts. The long mesas had been etched the same way as the short mesas and patterned for 4μm width and 4μm spacing (VH-44). The samples are shown in the table below

**Table 6-1.** A table showing the samples used in part II where mesa and contact size were varied.

| **Sample name** | | **Mesa size (μm$^2$)** | **contact size (μm)** | |
|---|---|---|---|---|
| | | | **width** | **spacing** |
| **Short mesa** | VH-48 | 30×12 | 4 | 8 |
| | VH-88 | 48×12 | 8 | 8 |
| **Long mesa** | VH-44 | 400×25 | 4 | 4 |
| | VH-44(2) | 400×25 | 4 | 4 |

## 6.4 Measurement

The measurement in part II used the transport measurement set-up that is described in chapter 2. The sample was mounted on the different insert that used in part I, which can orient the sample's surface parallel to the magnetic field.

### 6.4.1 Hall voltage

We first describe our geometry on the short mesa; a current is passed from the back contact on the substrate to the central electrode on mesa and the voltage is measured at the adjacent electrodes. Therefore the current is injected in vertical direction perpendicular to the voltage electrodes. The magnetic field is applied parallel to the surface of the devices. Figure 6.4.1 shows a diagram of the geometry used in this part.

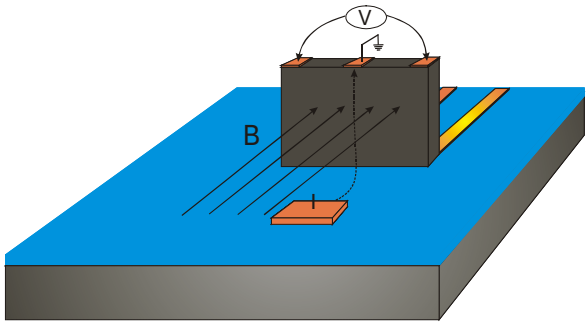



**Figure 6.4.1.** Figure showing the geometry studied. A current is injected from the back contact to the central electrode on the mesa and the voltage is measured across at electrodes on both sides. The magnetic field direction is parallel to the device surface.

For the long mesa, which has 13 electrodes with the same height as the 3 electrodes, we divided the Hall voltage measurement into 2 parts for investigation. The first part is substrate bias, which is the same as described for the short mesa. The second part is mesa bias, in which the current is applied only through contacts on the mesa, and the back contact is eliminated as shown in figure 6.4.2.

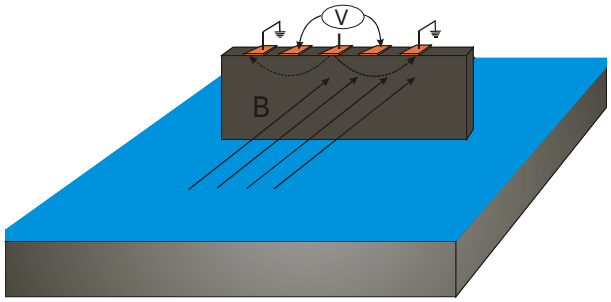



**Figure 6.4.2.** Illustration of Multi electrodes on a single mesa. The current is applied at the central contact and grounded at both ends of the mesa.

The magnetic field is applied parallel to the surface of mesa that is perpendicular to both current and voltage vectors.

### 6.4.2 Current dependence

To study the Hall voltage as a function of the applied current (chapter 7), a variable resistor box was used as a series resistor in figure 2.4.2. The applied current was 5, 10, 50 and 100μA.

### 6.4.3 Angular dependence

Angular measurements are made by rotating the sensors in a homogeneous field created by electromagnetic coils, instead of turning a permanent magnet. The study of the Hall resistance as a function of the angle between the field direction and the plane of the wafer is presented in figure 6.4.3.

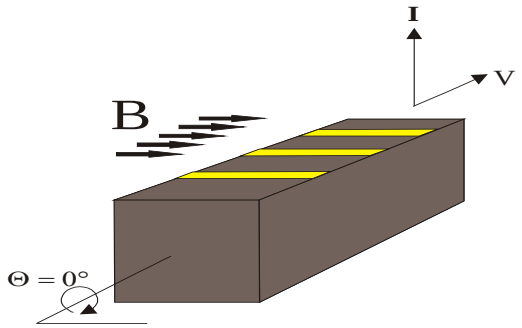



**Figure 6.4.3.** Angular dependence measurement. By rotating a sample in a constant magnetic field parallel to its surface around an axis parallel to voltage measurement direction.

A rotating insert has been used for this purpose; the stepping motor is used to control the rotating speed at 100 steps per minute. The rotation is obtained without discontinuity or dead angle over a full 360°

## 6.5 References

[1] R.S. Popovic, A vertical Hall device, *IEEE Electron Device Lett*, vol. EDL-5(9) (1984) 357

[2] R. S. Vanha, F. Kroener, T. Olbrich, R. Baresch and H. Baltes, *J. of Micro. Electro. Mecha*, vol.9, (2000) 82-87

[3] M.C. King, *VLSI Electronics*, Vol. 1. Eds. N.G. Einspruch, Academic, New York, (1981).

[4] J.H. Bruning, *Semiconductor Technology, Electrochemical* Soc, Eds. D.A. Doane, D.B. Fraser, D.W. Hess, Penningston, (1982).

[5] R. Williams, *Modern GaAs processing methods*, Artech House, Boston, (1990).

# Chapter 7

# Experimental results


7.1 Simple 3-electrode structures……126

*7.1.1 In-plane measurement*……..…126

*7.1.2 Current dependence*……..…128

*7.1.3 Angular Field dependence*…….……..……129

*7.1.4 Summary of the sensitivities of the VMHS*….……..……130

7.2 Multiple electrodes Concept……...….……..135

*7.2.1 The Hall voltage as a function of contact positions*……..……...….135

*7.2.1.1 Substrate bias (VMHSs)*……...…135

*7.2.1.2 Mesa Bias (VMHSm)*……139

*7.2.1.3 Discussion*……..……..……142

*7.2.2 Multiple VMHS on a single mesa*……..……143

*7.2.2.1 Substrate bias (VMHSs)*……144

*7.2.2.2. Mesa Bias (VMHSm)*……145

7.3 Multiple contacts and offset reduction……...147

7.4 Conclusions……151

7.5 References……..154

# 7. Experimental results

For our geometry, we report on how the implementation of in-plane Hall effect sensors allows for vertical current injection. The first group of samples are called short mesa structures, labelled VH-48 and VH-88, which have a mesa size of approximately $30\times12\mu m^2$ and $48\times12\mu m^2$, respectively. For the short mesa samples, we first measured the magnetic field dependence at room temperature with the field oriented along the expected direction of maximum sensitivity, and then the Hall voltages as a function of the applied current. The samples were then rotated in a constant magnetic field to observe the angular field dependence of the devices.

After examination of the basic characteristics of the Hall effect in a short mesa, we investigate a long mesa, sample VH-44, which has multiple contacts. The measurement consists of two stages to show that the long mesa with many contacts can be created as described below.

- A plot of the Hall voltage as a function of voltage contact positions
- Multiple VMHS on a single mesa that can operate independently

All of these long mesa measurements are studied in the case of the current injection from substrate to the mesa as well as current bias using only the mesa.

Finally, we show that the multiple contact design has the advantage that it can be used to decrease the offset voltage in our device.

## 7.1 Simple 3-electrode structures

The sensor chip was mounted on a non-magnetic package and placed into the magnetic fields of –0.3T<$B$<+0.3T at room temperature. The vector of magnetic flux is parallel to the chip surface, and perpendicular to the I-V plane.

### 7.1.1 In-plane measurement

The Hall resistance as a function of the applied magnetic field for current drive of VH-48 and VH-88 at 298K is displayed in Figure 7.1.1. For this section, a current of 100μA is injected from the substrate and flows through the central contact on the mesa. The voltage contacts are placed at the contacts adjacent to central one (see section 6.4.1).

The Hall resistances for constant current drive show non-linearity due to the significant magnetoresistance (MR) component which is present. We have separated the data into symmetric ($R_{\mathrm{sym}}$) and antisymmetric parts ($R_{\mathrm{antisym}}$) due to a significant contribution from magnetoresistance effects, which masks the excellent linearity of the Hall voltage.

$$R_{sym} = \frac{1}{2}\big(R(+B) + R(-B)\big)$$

$$R_{antisym} = \frac{1}{2}\big(R(+B) - R(-B)\big)$$

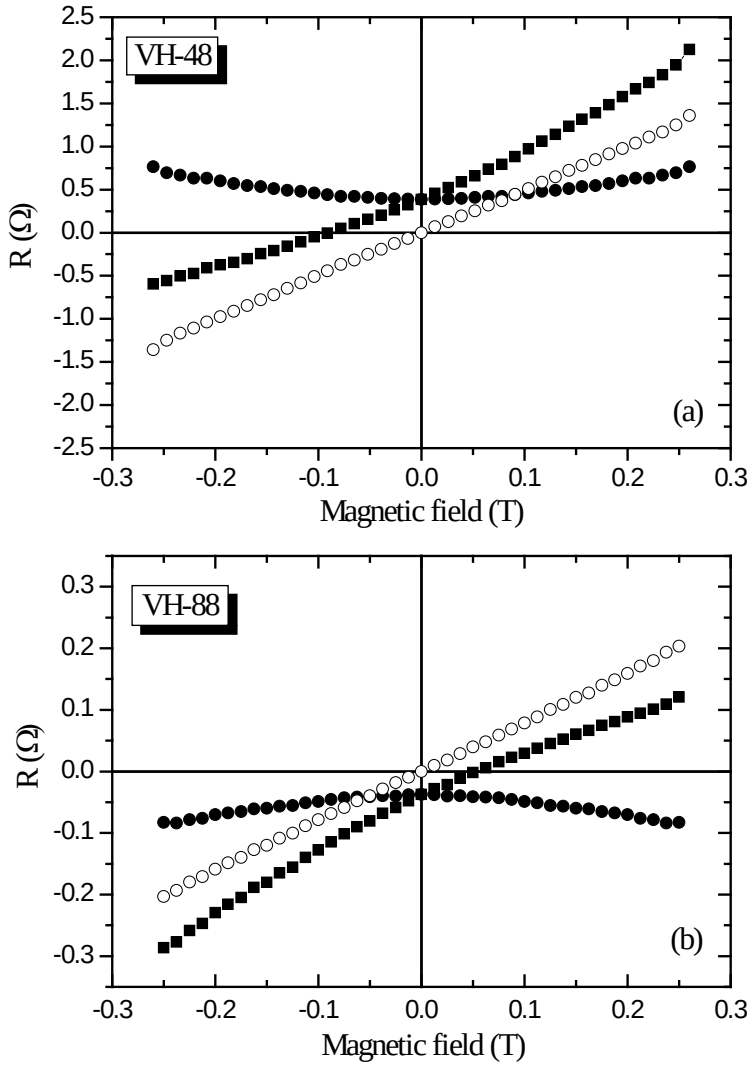



**Figure 7.1.1.** The Hall resistance (square) of the short mesa plotted against the magnetic field at room temperature. The current 100μA applied from the substrate to the central contact on the mesa. The data is separated into symmetric (filled circle) and asymmetric (open circle) parts.

The MR component is caused by an asymmetric current path, which is probably due to the current flow to contacts at the sidewall of the mesa, as the sidewall is not completely covered by the insulating layer.

### 7.1.2 Current dependence

One of the most important characteristics of a Hall sensor is the dependence of the signal on bias current. For our reported VMHS, we investigated the dependence of the sensitivity as a function of the applied drive current (5, 10, 50 and 100μA), these were done with a fixed magnetic field (figure 7.1.2.).

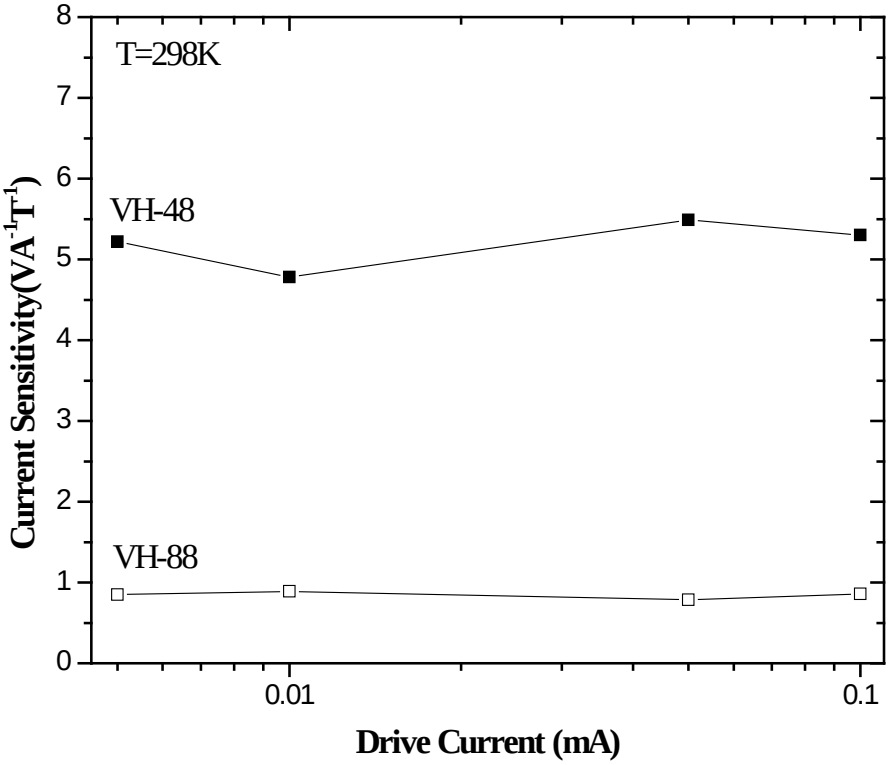



**Figure 7.1.2.** Sensitivity at 0.2T as a function of the applied drive current at room temperature.

The current sensitivities obtained from experiments, calculated by $\frac{R(B^+)-R(B^-)}{B^+-B^-}$. The data indicated an average current sensitivity of $5.20\pm0.42 VA^{-1}T^{-1}$ for VH-48 and a very low sensitivity $0.845\pm0.06 VA^{-1}T^{-1}$ for VH-88. However, the sensitivities for the current drive shown a linear response up

to I=100μA for both samples. This is corresponds to a current density of 29.76A/cm$^2$ for VH-48 and 20.8A/cm$^2$ for VH-88.

### 7.1.3 Angular field dependence

In order to check the operation of the device as a vertical Hall sensor, it is interesting to study the angular dependence of the devices. The angular measurements are made by rotating the sample in a constant magnetic field around the axis of the mesa as described in chapter 6.

The Hall resistance of VH-48 is plotted against the angle between the field direction and the plane of the wafer with the zero field offset subtracted. The absolute response of the sensor has maxima at θ=0° and 180° (when I and B are perpendicular) and is to a good approximation proportional to the cosine of the angle. Measurement of the peak amplitudes of 0.55Ω, 0.83Ω and 1.20Ω at 0.1, 0.15 and 0.2T respectively, as presented in Fig. 7.1.3, give sensitivities of 5.0-5.5Ω/T in agreement with the measurement above.

The angular dependence data show that the device is insensitive to the component of the magnetic field in the direction of the current as expected. The location of the maxima and minima also verifies that the average orientation of the current density is in the expected vertical direction. Sample VH-88 has also been measured; the amplitudes are very small due to the current sensitivity of the device being very low. However, the sensor shows the same angular dependence, with highest response when the magnetic field is normal to the I-V plane.

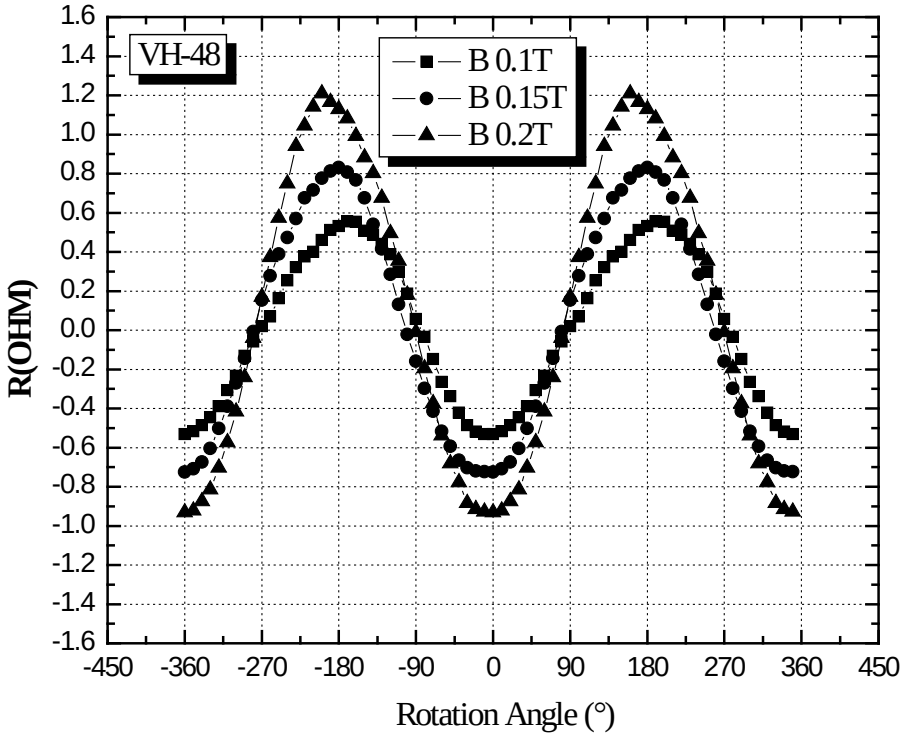



**Figure. 7.1.3.** Measured Hall voltage obtained from rotation in a field of 0.1, 0.15, 0.2T respectively. The amplitudes were subtracted with corresponding offset.

We have shown that we have succeeded to fabricate Hall effect devices on a length scale of microns. Our micro-Hall sensor has smallest dimensions ($l \times w \times d$) of 28μm ×12μm ×1.5μm. These are useful for the detection of magnetic fields produced by magnetic microstructures, such as the investigation of vortices in superconductors for fundamental studies. Hence, the VMHS can be optimised to achieve high current sensitivity by reducing either the width or the spacing of contacts in order to reduce the active region in our geometry.

### 7.1.4. Summary the sensitivities of the short mesa

Both the current and voltage sensitivities of Hall devices are strongly dependent on the properties of the materials and the geometrical parameters of the

structures studied. The length-to-width ratio ($\frac{l}{w}$) in the conventional rectangular geometry is equivalent to the ratio of $\frac{h_m}{l_v}$ in VMHS, which is usually very small. Ref[1] shows that the geometrical correction factor ($G_H$) is a function of the length-to-width ratio ($\frac{l}{w}$) and Hall angle. At very small ratios the geometrical correction factor varies linearly with $\frac{l}{w}$. In our geometry with the limit of $\mu B << 1$, we estimate $G_H = a\frac{h_m}{l_v}$ with $a$=0.76.

The voltage sensitivity depends on the resistance of the device, $S_v = \frac{S_I}{R}$, the mobility, the geometry of the sample and also the geometrical correction factor. So, to achieve high voltage sensitivity, high carrier mobility is required. From equation 5.3.3(b) by using $G_H$ equal to $0.76 \times \frac{h_m}{l_v}$ as before and the theoretical voltage sensitivities in small ($\frac{l}{w}$) are 3.34 $T^{-1}$.

To calculate the voltage sensitivities in our real device, we need to use the measured device resistances ($R_{mea}$). These resistances were 200Ω and 250Ω for VH-48 and VH-88 respectively. This is approximately 100 times larger than the expected value of about 1.5Ω for the mesa alone with perfect contacts. The expected values $R = \rho\frac{l}{A}$ are calculated from the parameters below:

i. The resistivity of the device which is $4.41 \times 10^{-5}$Ω.m.

ii. The length which is equivalent to the height of mesa ($l$=1.5μm).

iii. The area which is the metallic pad area that is used as the current contact ($A=12\times4\mu m^2$).

We also measured the substrate resistance ($R_{sub}$) by measuring the resistance between 2 back contacts and found that the back contacts are ohmic and the $R_{sub}$ (< 6Ω) is lower than $R_{mea}$. The voltage sensitivities ($S_v$), calculated from $\frac{S_I}{R_{mea}}$, are $0.0261T^{-1}$ and $0.0034T^{-1}$ for VH-48 and VH-88 respectively.

The explanation for the $R_{mea}$ being higher than expected is due to the imperfect attachment of the metal on the mesa surface. After $SiO_2$ coating and the lift-off processing, it is likely that some $SiO_2$ still remains on the mesa surface and this prevents the metal completely adhering to the surface, as illustrated in figure 7.1.4.

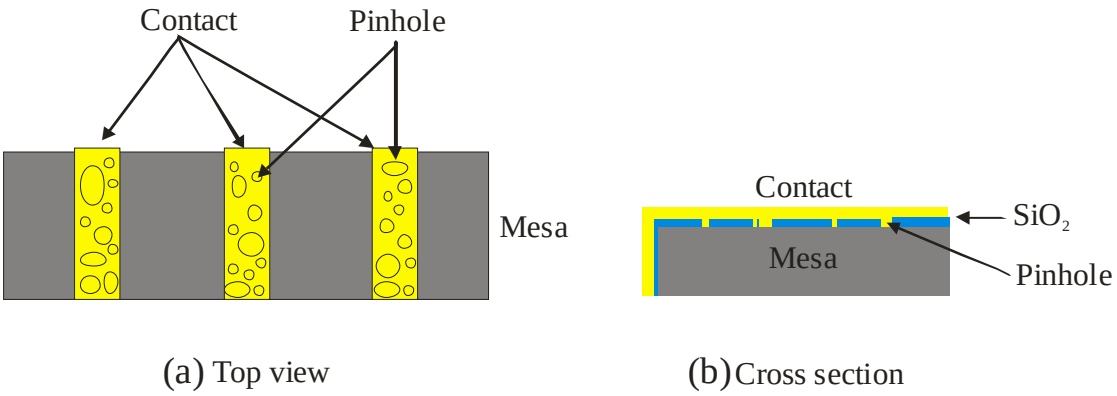
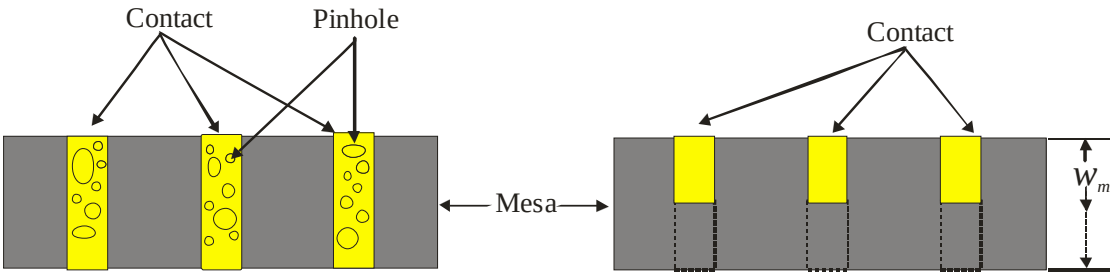



**Figure 7.1.4.** (a) The top view VMHS shows that contacts have an imperfect attachment on the mesa surface (b) the cross section of mesa shows the remaining $SiO_2$ layer that prevents the metal adhering completely to the mesa surface.

The remaining $SiO_2$ on the surface is pinhole-like, with only a small part of the metal attached perfectly to the surface so the contacting metallic area might

be much smaller. If this were of order $1\times1\mu m^2$, this would lead to values for $R_{mea}$ as high as those found experimentally.




(a) The imperfect attachment of contacts

(b) The total contact area without pin-hole area

**Figure 7.1.5** The top view of the mesa (grey area) with metallic contact (yellow area). (a) Showing the imperfect attachment of the contacts (with pinhole). (b) The equivalent total metallic area without the pinhole.

As described in section 5.4 the sheet density in our geometry has to be calculated by multiplying the bulk carrier density by the width of the mesa. Calculating from equation 5.3.3(a) using the appropriate material properties, a geometrical correction factor and a width $w_m$=12μm, predicts a current sensitivity of $0.927VA^{-1}T^{-1}$ for VH-48 and $0.773VA^{-1}T^{-1}$ for VH-88. As expected, higher sensitivity is obtained from the shorter length $l_v$. The magnitude of the experimental results, however, is higher than predicted by the theory. This is probably due to two causes:

(i) The diffusion of the gold contacts spreading under the mesa causing the length ($l_v$) to be shorter.

(ii) The imperfect attachment of the gold contact (figure7.1.4) causes the smaller contacting metallic area. The contacting metallic area without the pinhole area is equivalent to the shorter length of gold contact on the mesa

surface as illustrated in figure 7.1.5. Therefore the $w_m$ is shorter, leading to the $S_I$ in practical device to be much higher ($S_I = \frac{1}{new_m} G_H$) than the theory.

The current and voltage sensitivities are listed in table 7-1.

**Table 7-1** The sensitivities for the short mesa samples measured at room temperature (298 K).

| Sensor | Dimensions | | | $S_I$ ($VA^{-1}T^{-1}$) | | $S_v$($T^{-1}$) | |
|---|---|---|---|---|---|---|---|
| | $l_v$(μm) | $w_m$(μm) | $h_m$(μm) | Experiment | Theory | Estimated | Theory |
| **VH-48** | 20 | 12 | 1.5 | 5.2 | 0.927 | 0.0261 | 3.34 |
| **VH-88** | 24 | 12 | 1.5 | 0.845 | 0.773 | 0.0034 | 3.34 |
| **Ref[2]** | 21.5 | *t*=9 | *Depth*=3 | 18 | | 0.015 | |

We compare the sensitivities for our structure with Vertical Hall sensors (VHS) that have been fabricated using Silicon as reported in ref[2]. These devices were fabricated from a high-voltage CMOS process that provided a 3μm n-diffusion layer on the p-substrate. The plate thickness (*t*) was 9μm, which is equivalent to $w_m$ in our case, and the distance between voltage contacts was 23μm. The surface concentration was estimated to be about $2\times10^{16}cm^{-3}$. This device yielded a current sensitivity ($S_I$) of $18VA^{-1}T^{-1}$ and a voltage sensitivity ($S_v$) of $0.015T^{-1}$.

From equation 5.3.3(a), it can be seen that current sensitivity depends on the carrier concentration and geometrical parameters. Devices with a low carrier concentration (*n*), small width ($w_m$), and high geometrical correction factor ($G_H$) produce high current sensitivity. In comparing the values of these three factors between the two types of sensors, VHS from ref[2] have a lower *n*, smaller $w_m$ and higher $G_H$ than our devices, so in each of three factors that affect current

sensitivity, the Vertical Hall Sensor has a better value. The combination of these 3 factors enables the VHS from ref[2] to have higher current sensitivity ($S_I$) than the devices studied here.

A high mobility is essential for high voltage sensitivity $S_v$. InSb can be considered a good Hall sensor device because it exhibits a much higher mobility ($4.4m^2/Vs$) than Si ($0.15m^2/Vs$). The $S_v$ is calculated from the current sensitivity assuming that the device resistance is dominated by the mesa. As the mesa resistance is quite low (of order a few ohms) this means that the practical device performance is strongly influenced by any contact resistance which may be present. In our device, $R_{mea}$ were high due to the non-uniformity of attachment of the metallic pad, an error in the fabrication process. To improve the voltage sensitivity of devices studied here, the entire $SiO_2$ layer must be carefully removed from the mesa surface to allow perfect adhesion of the metal contact.

## 7.2 Multiple electrodes concept

In order to succeed in fabricating a VMHS, we have further generated a multi-electrode structure, which has 13 electrodes on a single mesa ($400\times25\mu m^2$) with the same height as the 3-electrode mesas. The multi-electrode sample allows us to study the effects of the current distribution. In this section, the Hall voltage is studied first as a function of contact position, and then for multi-VMHS. In each part contained tow biasing conditions which are the current is injected from the substrate to the mesa (substrate bias) and the current bias using only mesa contacts and the back contact is eliminated (mesa bias).

### 7.2.1 The Hall voltage as a function of contact positions

Using the short mesa, we have shown that our geometry is sensitive to magnetic fields parallel to the mesa surface. In many research groups, simulation has shown[2-5]that the current lines in such a vertical Hall-effect device are not straight, but rather strongly curved. In this section, we monitor the Hall voltage as a function of contact positions.

#### 7.2.1.1 Substrate bias (VMHSs)

The experiments were performed on a long mesa with contact width and spacing between contacts of 4μm and 4μm, respectively. Applying the current from a back contact on the substrate to the central contact on the mesa, we study the current and voltage distribution. The sets of voltage contacts were paired from contacts 6 and 8 to the end of the mesa, which are contacts 6 and 13, as indicated in figure 7.2.1. The sample was placed in fixed magnetic fields between zero and 0.1T at room temperature.

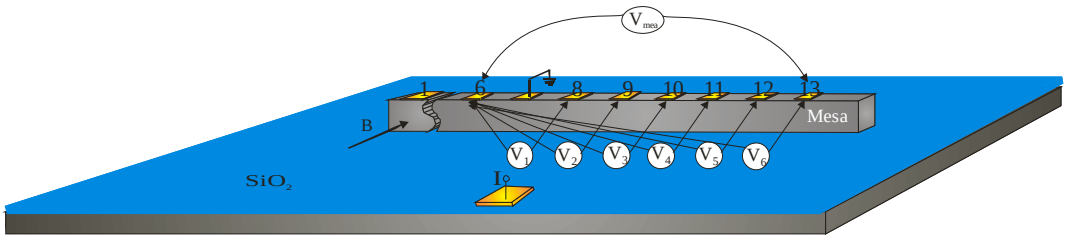



**Figure 7.2.1** The schematic presents one side of the long mesa with multi-electrodes on the top. The current of 100μA is injected from the back contact on the substrate to the mesa. The in-plane Hall voltages are measured between the set of paired voltage contacts. The magnetic field is applied parallel to the sample surface.

The first voltage ($V_1$) was measured between the sensing contacts 6 and 8 while the current was injected from the substrate contact and grounded at contact 7, which is on the mesa. The second voltage ($V_2$) was measured using the same sensing contact on one side and moving the second contact further along the bar with the same biasing current condition. This process is repeated with voltages $V_3$, $V_4$, $V_5$ and $V_6$ measured from fixed contacts 6 and 10, 11, 12 and 13 respectively. The voltage differences are measured at B=0 and B=0.1T for different sensing contacts as listed in table 7-2.

**Table 7-2** The voltages are measured from different voltage contact pairs on the long mesa samples with and without magnetic field. The biasing current condition is substrate bias.

| Contact pair no. | | Voltage (μV) | | δV(μV) | $S_I$ (V/AT) |
|---|---|---|---|---|---|
| | | B=0 | B=0.1 T | | |
| 6 | 8 | 0.8 | 2.15 | 1.35 | 0.135 |
| | 9 | 0.38 | 1.5 | 1.12 | 0.112 |
| | 10 | -0.48 | -0.03 | 0.45 | 0.045 |
| | 11 | -1.78 | -1.45 | 0.33 | 0.033 |
| | 12 | -2.35 | -2.22 | 0.13 | 0.013 |
| | 13 | -3.66 | -3.6 | 0.06 | 0.006 |

It is shown in the table that the measured voltages vary from 0.8μV to -3.66μV at B=0 and 2.15μV to –3.6μV at B=0.1T. The Hall voltage (δV) decreases as the separation of the outer voltage contacts from the current injection point is increased as plotted in figure 7.2.2.

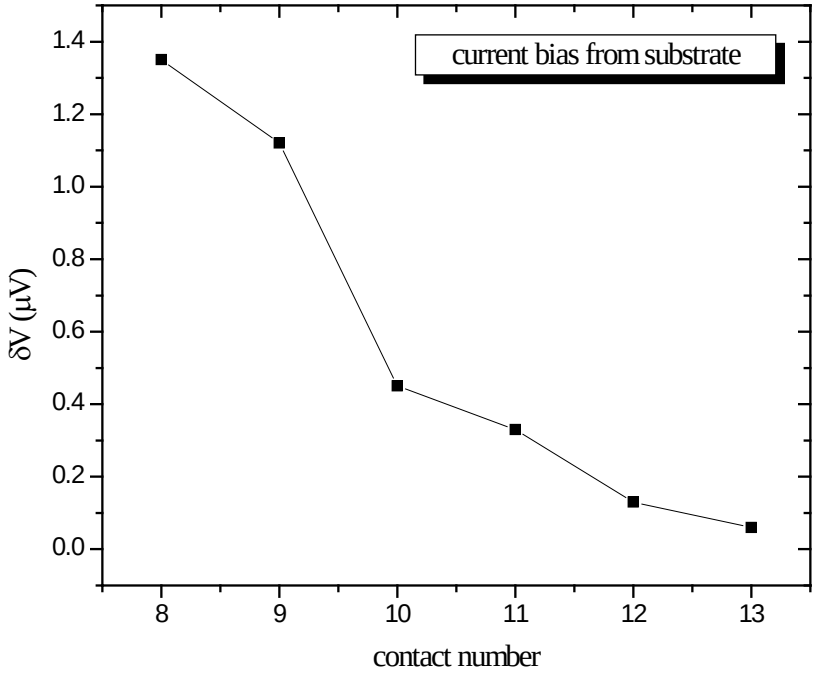



**Figure 7.2.2** The Hall voltage measured from different contacts on the mesa. (Current drive 100μA, at B=0.1T)

The Hall voltages in this section are measured on the same mesa, but the measured regions that produce Hall voltages are different. We varied the contact position along the mesa so that the difference in each region is the length as illustrated in figure 7.2.3. As described earlier the width and spacing of contact give the shortest lengths between 2 voltage contacts as 16μm, which is the smallest VMHS ($A_1$) in sample VH-44 and generates the $V_1$. With the same current contacts, the second measured region has length 24μm, and the rest are shown in the figure. The highest sensitivity is obtained from the smallest region ($A_1$), and is 0.135V/AT. Sensitivity decreases as the active regions are increased, as listed in the last column of table 7-2.

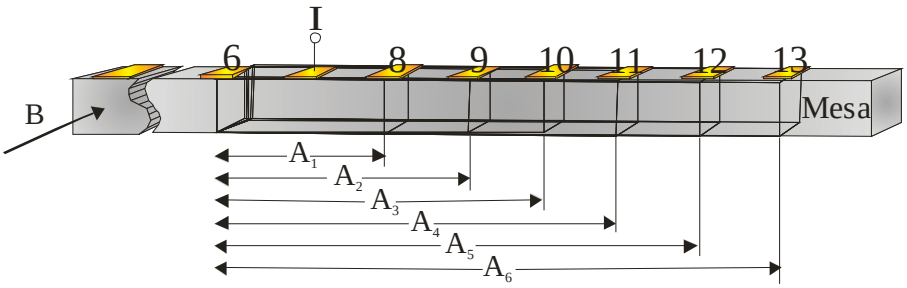



**Figure 7.2.3** Illustration of the active regions used to measure the Hall voltages. $A_1$ has a length of 16µm and $A_2$, $A_3$, $A_4$, $A_5$ and $A_6$ have lengths 24, 32, 40, 48, and 56µm, respectively.

The decrease of Hall voltage while the active region increases is discussed later. Our next motivation with the VMHS concept is to create a Hall sensor on a vertical mesa without the need for a back contact on the substrate.

### 7.2.1.2 Mesa Bias (VMHSm)

The measurements in this section use the same sample to investigate the Hall voltage using current injection through the mesa. The current is injected at the central contact and flows through the mesa in the direction of the external contacts at both ends of the mesa as illustrated in Figure 7.2.4. The voltage measurements in this section use the same contact pairs as measured in the previous section, but there are 5 measurements ($V_1$-$V_5$) observed. The number of voltage contacts is reduced because two contacts on the mesa have to be negative current contacts.

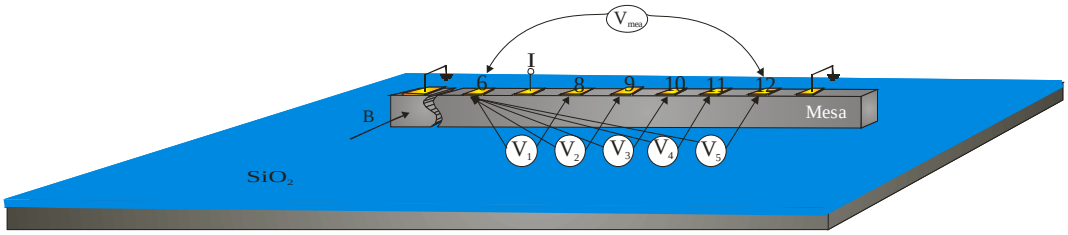



**Figure 7.2.4** The schematic presents one side of a long mesa with multi-electrodes on the top. The 100μA current is injected from the central contact and grounded at the both ends of the mesa. The in-plane Hall voltages are measured between the set of paired voltage contacts. The magnetic field of 0.1T is applied parallel to the sample surface.

To measure the Hall voltage, the sample is placed into the magnetic field, which is parallel to the mesa surface. The measured voltages for magnetic field of 0 and 0.1T are listed in table 7-3. The values of voltage vary from –0.6μV to 3.4μV for B=0T and –2.05μV to 3.31μV when the sample is placed in a magnetic field. The Hall voltages (δV) are calculated from the sample voltages taken with and without magnetic field.

**Table 7-3** The Hall voltages are measured from different contact pairs on the long mesa samples with and without magnetic field. The biasing current condition is mesa bias.

| Contact pair no. | | Voltage (μV) | | δV (μV) | $S_I$ (V/AT) |
|---|---|---|---|---|---|
| | | B=0 | B=0.1T | | |
| 6 | 8 | -0.6 | -2.05 | 1.45 | 0.145 |
| | 9 | -0.4 | -1.51 | 1.11 | 0.111 |
| | 10 | 1.21 | 0.49 | 0.72 | 0.072 |
| | 11 | 2.4 | 1.83 | 0.57 | 0.057 |
| | 12 | 3.4 | 3.31 | 0.09 | 0.009 |

The Hall voltage plotted in Fig. 7.2.5 shows that the Hall response remains basically dependent on the voltage contact position as was observed in the substrate bias case (figure 7.2.2).

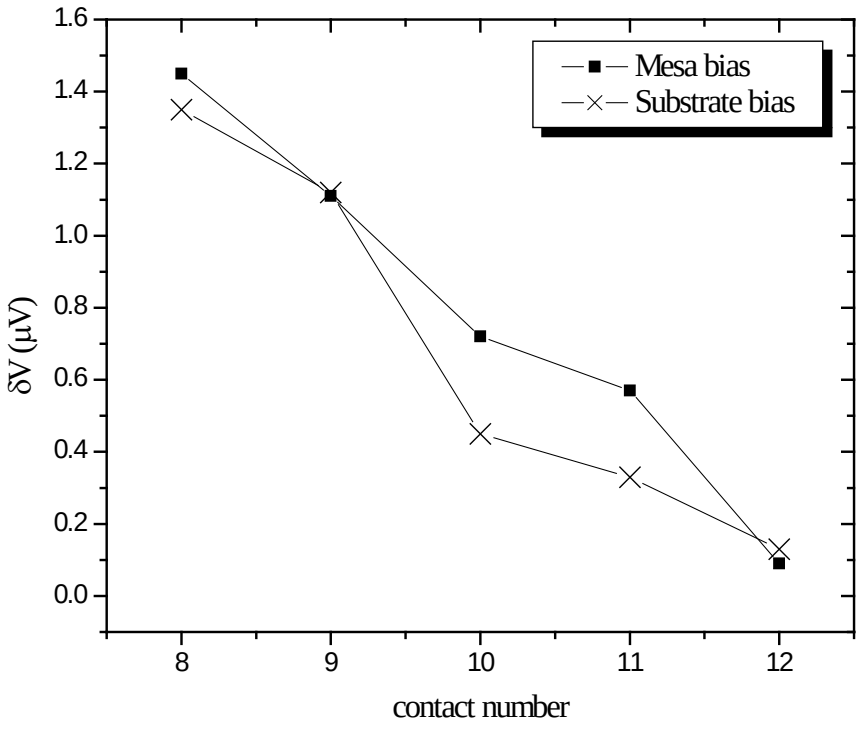



**Figure 7.2.5** The comparison of Hall voltage measured from different contact number of the mesa bias (filled square) and substrate bias (cross), with the current drive of 100μA, at B= 0.1T.

However comparison with the mesa bias case shows that the sensitivity, and hence the current density, is somewhat more widely spread than for the substrate bias configuration, as schematically shown in figure 7.2.6.

The cause of this is the different current distribution. It is likely that in the first case, the clustered current flows between top and substrate contacts, whereas in the second case it flows below the mesa surface in the direction of the external current contact.

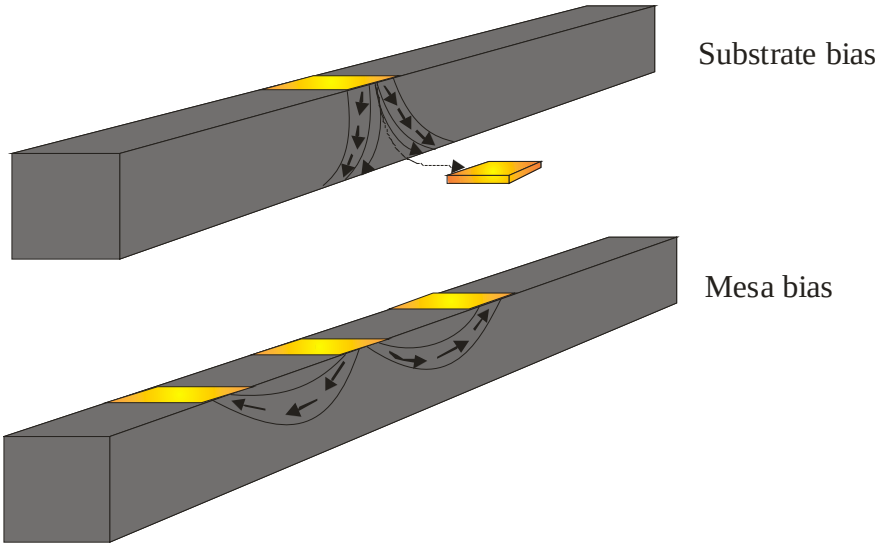



**Figure 7.2.6** Schematic presentation of the current distribution in mesa and substrate bias condition.

Significantly, however, the creation of VMHS without current injection from a back contact has been achieved, implying that the total device area can be reduced to a smaller size, where the substrate is no longer necessary.

### 7.2.1.3 Discussion

The Hall voltage measured in both cases in the long mesa is smaller when the voltage contacts are moved to wider separations as shown in sections 7.2.1.1 and 7.2.1.2. Additionally, tables 7-2 and 7-3 show that an increased magnetoresistance component is found. The cause of this behaviour can be explained by mapping the structure to a triangular model as shown in figure 7.2.7.

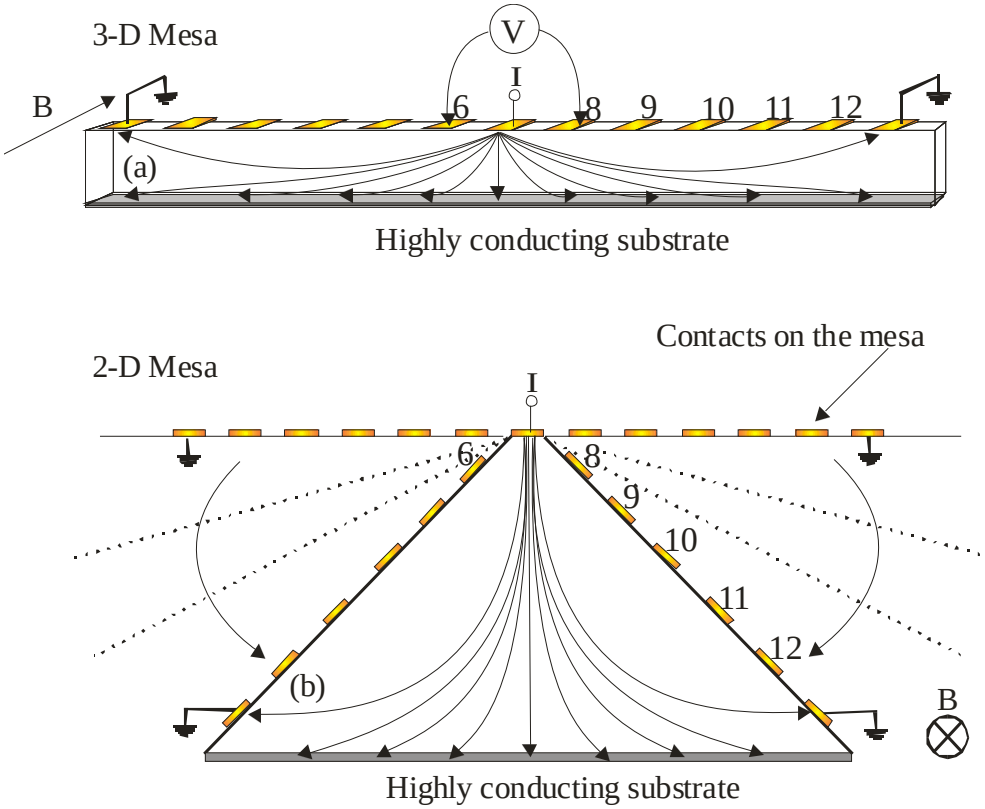



**Figure 7.2.7** Schematic representation of the long mesa sample. (a) The 3-D long mesa sample with all contacts on the mesa surface; a magnetic field is applied parallel to the mesa surface. (b) 2-D of long mesa sample. All contacts are on the perimeter of triangle and the base of the triangle is a high conducting substrate denoted by grey colour; magnetic field is applied perpendicular to the diagram. Lines represent the current distribution.

Our long mesa samples are fabricated from InSb which is a highly conducting semiconductor material. To describe the cause of the decrease in Hall voltage and increasing MR effect in the long mesa sample, we now consider it as a triangular shape, as illustrated in figure 7.2.7(b). All contacts on the mesa are on the perimeter of the triangle. The central current contact on the mesa is placed at the top of the triangle. Both arms of the mesa are tilted so that the ground current

contacts are close to the base of the triangle, which is the highly conducting substrate.

To compare the measurements between the long mesa and the triangular model, the voltage is measured from different contacts. We move the contact to the longer position (contacts 8 to 12) in the long mesa. This is similar to when we move the voltage contact, where the contacts are progressively closer to the highly conducting area at the base of the triangular model. Both geometries have a similar current distribution. The largest current density is found at the shortest distance in a long mesa as similar as at the upper region of the triangular model. When the voltage is observed at the contacts farthest away from the injecting contact, and also at the wider region at the base of the triangle the current density becomes smaller. The Hall voltage does not appear at longer voltage contact separations (also at the bottom of the triangle) because the circuit shorted by the highly conducting area.

### 7.2.2 Multiple VMHS on a single mesa

The fabrication process can easily mount many electrodes onto the mesa. It is also possible to use the multiple contacts on the bar to create a multiple VMHS on a single mesa, which may be used, for example, for magnetic field profiling or gradient detection.

### 7.2.2.1 Substrate bias

Sets of 3 adjacent current and voltage contacts were studied with the set of 3 contacts being moved successively along the bar as shown in Figure 7.2.8. The first investigation uses the substrate bias conditions.

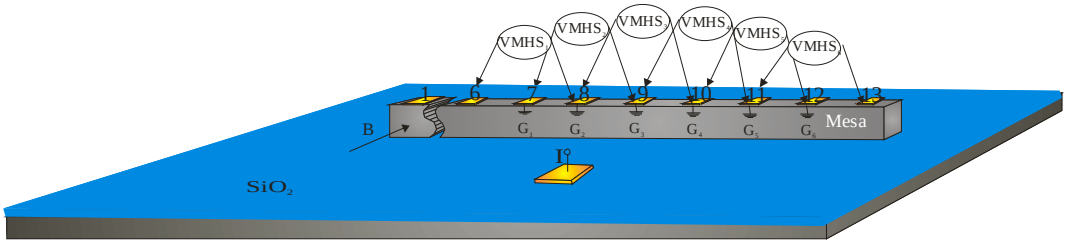



**Figure 7.2.8** Illustration of multiple VMHS on a single mesa, by using the set of the shortest distance of voltage contact and a corresponding ground current contact ($G_1$-$G_6$) to create each single VMHS. The current is injected from the back contact.

The Hall voltage at 0.1T measured from the individual VMHS, gave values from 1.01μV up to 1.48μV, which indicates significant uniformity problems in the fabrication (the 4$^{th}$ VMHS apparently showed a shorted contact). The Hall voltage generate from individual VMHS are listed in table 7-4.

**Table 7-4** The Hall voltages measured from individual VMHS. Using a 100μA current drive from substrate to the mesa and placed in a magnetic field of 0.1T at room temperature.

| VMHS | Pin number | | Voltage (μV) | | |
|---|---|---|---|---|---|
| | Current | Voltage | B=0 | B=0.1T | δV |
| 1 | 7 | 6-8 | 0.85 | 2.16 | **1.31** |
| 2 | 8 | 7-9 | 0.34 | 1.82 | **1.48** |
| 3 | 9 | 8-10 | -0.6 | 0.41 | **1.01** |
| 4 | 10 | 9-11 | -0.42 | -0.6 | **0.18** |
| 5 | 11 | 10-12 | 0.22 | -1.17 | **1.39** |
| 6 | 12 | 11-13 | -2.2 | -3.35 | **1.15** |

The different values of the Hall voltage in these measurements are related to imperfections in the fabrication process, as the insulating layer is non-uniform over a significant area. These prevent a constant Hall voltage being generated.

### 7.2.2.2. Mesa bias

In our investigation of the Hall voltage in section 7.2.1, we found that the mesa bias (VMHSm) may be more advantageous than the substrate bias (VMHSs). The reason is that the current path in this case will flow only in the mesa, which removes the additional resistance from the substrate contact.

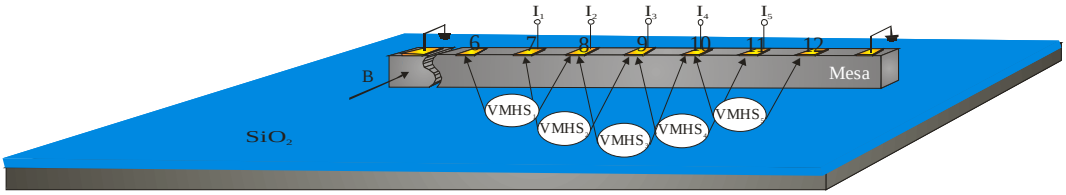



**Figure 7.2.9** Illustration of multiple VMHS on a single mesa, by using the set of the shortest distance of voltage contact with a corresponding positive current contact to create each single VMHS. The ground current contacts are on both ends of the mesa.

The current is now injected by using contact 7, 8, 9, 10 and 11 for VMHS 1-5 respectively; the negative current contacts are grounded at both ends of the mesa. Adjacent pairs of contacts were used to measure the Hall voltage as shown in figure 7.2.9.

The results show that the Hall voltages from an individual VMHS vary from about 1.17μV up to 1.38μV with exception of the fourth VMHS which apparently showed a shorted contact.

**Table 7-5** The Hall voltages are measured from individual VMHS. Using a 100μA current drive only on the mesa and placed in a magnetic field of 0.1T at room temperature.

| VMHS | Pin number | | Voltage (μV) | | |
|---|---|---|---|---|---|
| | Current | Voltage | B=0 | B=0.1T | δV |
| 1 | 7 | 6-8 | -0.69 | -2.07 | **1.38** |
| 2 | 8 | 7-9 | -0.23 | -1.40 | **1.17** |
| 3 | 9 | 8-10 | 0.68 | -0.52 | **1.20** |
| 4 | 10 | 9-11 | 0.88 | 1.01 | **0.13** |
| 5 | 11 | 10-12 | 0.39 | 1.71 | **1.32** |

From comparison of VMHSs and VMHSm in the case of multiple VMHS on a single mesa, it appears that the Hall voltage shows some small differences as can be seen in tables 7-4 and 7-5. Using both substrate and mesa bias, the Hall voltages produced in individual VMHS in this section are comparable to the Hall voltages obtained in section 7.2.1 when using the shortest distance between voltage contacts. The Hall sensitivities show that the VMHSm case would be appropriate for IC applications as the substrate contact can be removed.

## 7.3 Multiple contacts and offset reduction.

Hall sensors are used in a variety of applications to measure static and dynamic fields. A major drawback of these sensors is their offset voltage as exhibited in our samples. The offset voltage of a Hall sensor is usually due to the mixing of a small component of the magnetoresistance into the voltage measured by the Hall probes due to the errors in the geometry or homogeneity of the segment. The symmetry of a Hall sensor is never perfect: there are always small errors in geometry and contact resistance. Several methods have been introduced to decrease the offset voltage. A well-known technique to reduce the offset of Hall

sensors is the so-called spinning current technique.[6-11]However, this requires additional electric circuitry to drive the rotating current.

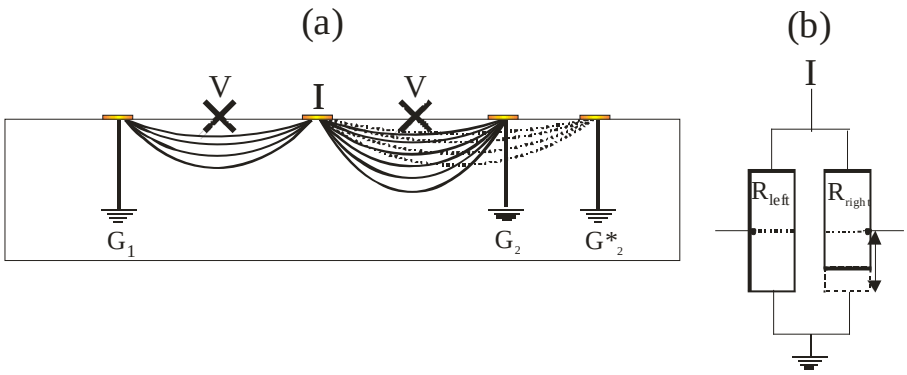



**Figure 7.3.1** Cross-section of the long mesa. (a) Layout of VMHS with multi-electrodes and (b) the corresponding equivalent circuit with two resistors. Current is applied from the central contact and grounded at both ends. The solid lines show an asymmetry of the current distribution. The ground contact can be moved to position $G^*_2$ to rebalance the resistor (dash lines)

Our earlier works shown that in the VMHS studied here there is a high offset voltage, and significant offset reduction is required. In this section we demonstrate that the offset can be controlled by moving the ground contacts to adjust the current distribution under the mesa surface. This structure can be described by an equivalent circuit consisting of two ohmic resistors, as displayed in figure 7.3.1.

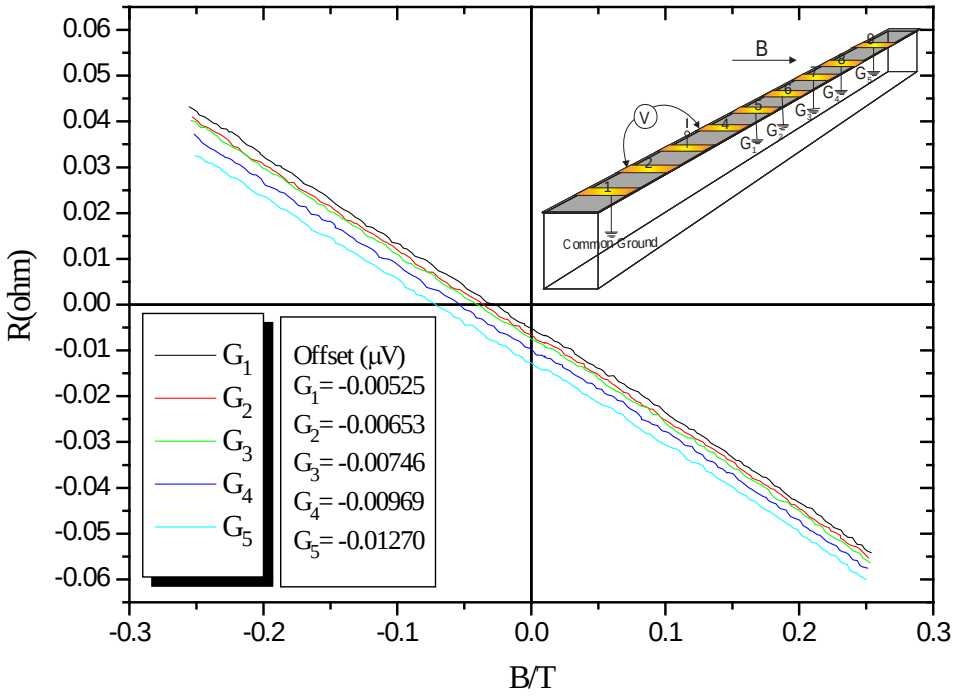



**Figure 7.3.2** The first investigation ($V_{24}$) for offset reduction of the long mesa sample VH-44(2). The position of ground contacts has been varied. The figure shows possibility of tuning the initial offset of the device to zero. Inset shows the picture of the offset reduction measurement.

The cause of the offset may be due to asymmetries in either the location of the Hall probes relative to the current-injecting contact, or asymmetries in the current flow to left or right. Figure 7.3.1 shows that the device may be considered as a bridge circuit. It shows in principle that it would be possible to adjust the device to zero offset by adjusting the current in the two arms of the circuit. This can be achieved by compensating the smaller resistor by increasing the length of the ground contact ($l_{left} < l_{right}$) to obtain ($IR_{\text{left}} = IR_{\text{right}}$), and then the offset voltages will be reduced.

In this section we used sample VH-44(2), which has the same contact width and spacing as sample VH-44. The first investigation $V_{24}$ used in this

section has the central current contact on pad 3 and the voltage contacts at the shortest distance, which is between pad 2 and 4. The fixed or common ground contact is on pad 1 and the first ground is on pad 5 for a symmetrical measurement. The initial offset observed in this pattern is very large (-0.00525μV). The second offset is measured by moving the ground contact on pad 5 further along the bar to pads 6, 7, 8 and 9, which are labelled as $G_2$, $G_3$, $G_4$ and $G_5$ respectively. We found that the offsets in these measurements are bigger. The different ground connections with corresponding offset voltages are listed in the table inset of figure 7.3.2.

It is clear that this sample has an imbalance of resistors on two arms even when the voltage contacts are symmetrical. The first investigation $V_{24}$ shows that we have to compensate the resistor on the left as all offset voltages are below the origin. By moving the observed voltage contacts to the right, the equivalent resistors will be equal. The measured Hall voltages will be shifted above the origin and the offset will be diminished.

The second investigation $V_{46}$ studied used the central current contact on pad 5 with the voltage measured between pads 4 and 6. The common ground is fixed at pad 3 and the first ground or earth contact for this pattern is on pad 7. The earth contacts are moved successively along the mesa to pads 8 and 9 to measure the Hall voltage, and we expect that they will be shifted above the origin.

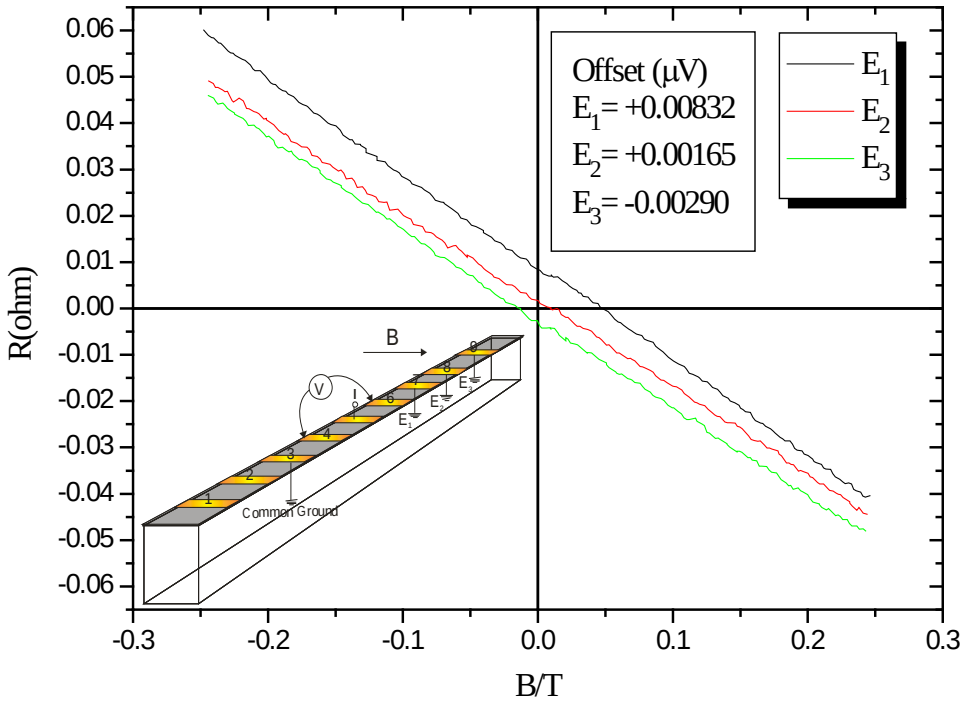



**Figure 7.3.3** The second investigation ($V_{46}$) for offset reduction of long sample VH-44(2). The observed contacts are moved to the right, where the central current contact is on pad 5 and measured voltage contacts on pads 4 and 6. The earth contact is varied along the mesa with a common ground fixed on pad 3.

The Hall voltage of $V_{46}$ is shown in figure 7.3.3. The initial offset measured by $E_1$ is 0.00832μV as expected, which is a positive. The second offset $E_2$ is smaller and almost reaches a zero-offset (0.00165μV). The final offset observed is for the longest earth contact $E_3$ and has an offset voltage lower than origin. All the offset voltages are listed in the inset table of figure 7.3.3.

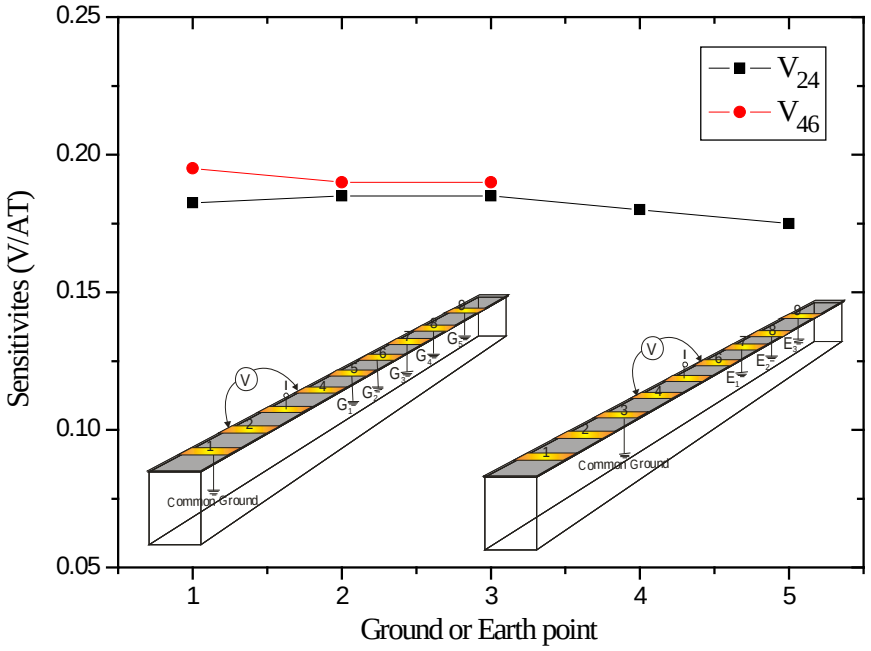



**Figure 7.3.4** The sensitivities of sensors produced from long mesa sample VH-44(2) measured from different voltage contacts. Squares present the sensitivities of $V_{24}$. Circles present the sensitivities of $V_{46}$ at room temperature between -0.25T >*B* >+0.25T.

The sensitivities of all observations in this section are almost constant due to the fact that the voltage contacts are fixed so the active region in the long mesa has the same dimension. The sensitivities measured from $V_{24}$ are 0.181±0.005 $VA^{-1}T^{-1}$ and $V_{46}$ are 0.193±0.002 $VA^{-1}T^{-1}$ as shown in figure 7.3.4. Finally, the sensors produced in this measurement show an excellent linearity up to 0.3T. Magnetoresistance effects are not detectable.

## 7.4 Conclusions

To conclude, we have studied the Vertical Mesa Hall Sensor (VMHS). This sensor geometry has been realized using a conventional lithographic process. Our results show a current sensitivity of 5.20 ± 0.42 $VA^{-1}T^{-1}$ for short sample VH-

48, which has a mesa size of $30\times12\mu m^2$, and a current sensitivity of 0.845± 0.06 $VA^{-1}T^{-1}$ for short sample VH-88, which has a larger mesa size of $48\times12\mu m^2$. These sensitivities are slightly higher than the values obtained from the calculations due to the gold contacts possibly spread under the mesa causing the length ($l_v$) to be narrower. Since the length-to-width ratios, $\frac{h_m}{l_v}$, in our geometry are very small, we thus estimated that $G_H = a\frac{h_m}{l_v}$, with $a$=0.76. The voltage sensitivities ($S_v = \frac{S_I}{R_{mea}}$) in practical devices are $0.0261T^{-1}$ with $R_{mea}$=200Ω for VH-48 and $0.0034T^{-1}$ with $R_{mea}$=250Ω for VH-88. $R_{mea}$ is high in real devices due to the non-uniformity of the attachment of the metallic pad.

By rotating the VMHS in a fixed magnetic field around the axis defined by the voltage contacts, we have shown that the device shows a good angular selectivity for the component of the magnetic field precisely in the plane of the wafer.

We have also shown an example of a multi-electrode VMHS, using 13 electrodes on a single long mesa. We have observed the Hall voltage as a function of the sensing contact positions. The Hall voltages are generally reduced for longer positions in all bias conditions that mean the smallest contact distances are preferred. The reduction of Hall voltage and the appearance of MR effect were explained by the triangular model.

In addition, we have further examined practical multiple VMHS on a single mesa by measuring a set of 3 adjacent current and sensing contacts. The Hall voltages from the individual VMHS are between 1.01-1.48μV using the

substrate bias condition, and between 1.17-1.38μV using the mesa bias condition. The different values are found due to imperfections of the fabrication process.

Finally, an existing problem of the Hall sensor is an offset in zero magnetic field. We used the advantage of the multi-electrode VMHS design to obtain very low offsets without any additional circuitry. Zero offsets can be achieved for these sensors. The sensitivities obtained from this measurement are slightly different and the Hall voltages are linear with magnetic field up to 0.3T.

However, we found that the insulating layer $SiO_2$, which we evaporated on an etching substrate, tends to be a pillar-like structure, leaving pinholes in between. These can provide an ohmic conduction path, which leads to shorting of the injection current and a reduction of the device sensitivity while the remaining $SiO_2$ on the mesa surface causes imperfect attachment of the metal pad, leading to high $R_{mea}$. Successful implementation of this geometry for practical devices will require significant improvement in the performance of the insulating layer on the substrate and the entire insulating layer must be removed from the mesa surface to allow the perfect metallic adhesion.

## 7.5 References


[1] R. S. Popovic, *Hall effect Devices*, 2nd edition, Institute of Physics Publishing, p198.

[2] Ch. Schott, P. -A. Besse, R. S. Popovic, *Sensors and Actuators A*: Physical, Volume 85, Issues 1-3, 25 August 2000, Pages 111-115

[3] R.S. Popovic, A vertical Hall device, *IEEE Electron Device Lett*, vol. EDL-5, p. 357, Sep 1984.

[4] A. M. J. Huiser and H. P. Baltes, *IEEE Electron Device Lett*, vol. EDL-5, No. 11, 482.

[5] E. Schurig, M. Demierre, C. Schott and R. S. Popovic, "*A vertical Hall device in CMOS high-voltage technology*", Sensors & Actuators A: 3184 pp. (2002)1-7.

[6] P.J.A Munter, *Sensors and Actuators* A21-23 (1990) 743-746

[7] P.J.A Munter, *Sensors and Actuators* A25-27 (1991) 747-751

[8] R. Steiner, Ch. Maier, M. Mayer, S. Bellekom, H. Baltes, *J. Microelectromech. Syst*. 8(4) (1999) 466-472.

[9] R. Steiner, Ch. Maier, A. Haberli, F.P. Steiner, H. Baltes, *Sensors and Actuators* A66 (1998) 167-172

[10] Sandra Bellekom, P.M. Sarro, *Sensors and Actuators* A66 (1998) 23-28.

[11] E. Schurig, C. Schott, P.A. Besse, M. Demierre, R.S. Popovic, *Sensors and Actuator*s A 110 (2004) 98-104.

# Chapter 8

# Summary of the thesis and future works

8. Summary of the thesis and future works…..…….157

8.1 Summary the accomplishment of the devices……..……....157

8.2 Future works...……..160

8.3 References……161

# 8. Summary of the thesis and future research

We have described the effort to study magnetotransport properties in a new geometry of magnetoresistance (MR) sensors in part I and the Vertical Mesa Hall Sensors (VMHS) in part II. As the conclusion chapter of this thesis, we conclude what progress was achieved in this thesis and comment on the existing problems for further research.

## 8.1 Summary the accomplishment of the devices

We summarise the achievements of the devices in this thesis by summarizing the main points in each part.

### Part I. The magnetoresistance sensors

First of all, as discussed in chapter 1, the samples in this part used the InAs/GaSb system to fabricate the semiconductor mesa, which was patterned with several metallic designs. Using the metallization process the metal was diffused into the active layer (InAs) to form the metal/semiconductor interface needed to influence the magnetoresistance effect in various geometries. The achievements from these main metallic patterns are:

1. Rectangular metallic pattern
    - This symmetric pattern showed both asymmetric and symmetric MR behaviour when combined with asymmetric and symmetric probe configurations respectively. In particular, the MR from asymmetric

probes is higher than the corresponding maximum for symmetric probes.[1]

- The sample with the smallest semiconducting area exhibits the largest MR effect.

2. Triangular metallic pattern
    - The asymmetric pattern generated asymmetric MR behaviour even though measured by a symmetric probe configuration.
    - The asymmetric MR shows a high sensitivity at B=0, i.e., the gradients $(\frac{dR}{dB})$ are high compared to symmetrical MR.
    - Both theory and experiment showed that decreasing length A resulted in a strong increase in magnetoresistance.
3. Tip metallic pattern
    - This combination of the asymmetric and symmetric patterns could exploit both asymmetric and symmetric MR behaviours.
    - This pattern shown the best performance judged by: the highest change in relative resistance $(\frac{R(B_{\max})}{R_{\min}})$ when combined with the inner probes. The highest absolute sensitivity $(\frac{dR}{dB})$ was found when using the outer probe configuration.
    - The important segment is the semiconducting gap area because the current distribution in the bulk of metallic area is relatively unimportant as we showed by the theoretical calculation that square and rectangular geometry with the same metallic pattern showed approximately the same MR effect.

## Part II. The Vertical Mesa Hall Sensors (VMHS)

The second part concerned a Hall effect sensor produced from bulk InSb material which is the highest mobility semiconductor near room temperature. The current flows through the etched mesa in the vertical direction, which allowed the sensors to measure the magnetic field parallel to the wafer surface. We can draw a number of important conclusions:

1. Short VMHS
    - Detection of a magnetic field in the plane of the wafer has been demonstrated to be possible using the proposed geometry and the sensitivities are linear in response up to 100μA.
    - The devices show a good angular selectivity for the component of magnetic field in the plane of the wafer.
    - Micro-Hall sensors have been successfully fabricated with the smallest dimensions ($l \times w \times d$) of 28μm ×12μm ×1.5μm.
2. Long VMHS
    - We have successfully produced multi-electrode VMHS, with 13 contacts on a single long mesa.
    - Elimination of the back contact on the substrate was achieved by driving the current only in the mesa.
    - The Hall voltage decreased for the more widely separated contact positions.
    - Multiple VMHS were produced on a single mesa that can measure local magnetic field independently.

- The multi-electrode design on a single mesa has been used to reduce the offset Hall voltage caused from the initially imbalance of resistances on both sides of the mesa.

## 8.2 Future works

This thesis has started the investigation of transport in a new geometry of magnetoresistance and vertical Hall devices. There are still some problems left to be solved and developed, which offer opportunities to carry on further research in these geometries.

The biggest challenge for EMR structures in the past few years is to use the geometry as an ultra-high density read-head sensor in recording media.[2] The high density can be accomplished by reducing the dimension of the sensors, as the density of the media is inversely proportion to the dimension. This requires further work to fabricate devices in a mesoscopic scale. When moving to mesoscopic devices, the most important future measurement would be an investigation of the resistance between the semiconductor and metal at the interface. This interface resistance has been studied in other materials, and it has been shown that the device performance is best if the interface resistance is low.[3]

For the VMHS, we proved that this geometry could operate as Hall sensors with the applied current in the vertical direction. As we described earlier the sensitivities depend on the geometrical parameters, which means that we can improve the sensitivities by increasing the current path in the vertical mesa (the mesa edge as high as possible). However we had a problem to make the gold connected at the sidewalls of the mesa, which can be a problem when the mesa edges are very high. The second improvement is the insulating layer as we had a moderate breakdown

voltage so the higher quality-insulating layer is required. The cleaned mesa surface is also important to achieve the perfect ohmic contact ($R_{mea}$ is lower).

## 8.3 References


[1] Zhou,-T.; Hines,-D.-R.; Solin,-S.-A., *Applied-Physics-Letters*. 29 Jan. 2001; 78(5): 667-9.

[2] S.A. Solin, D.R. Hines, J. S. Tsai, Y. A. Pashkin, S. J. Chung, N. Goel, and M. B. Santos, *IEEE Trans. Magn*. 38, 89(2002).

[3] Moller,-C.-H.; Grundler,-D.; Kronenwerth,-O.; Heyn,-C.; Heitmann,-D., *Journal-of-Superconductivity*. Feb. 2003; 16(1): 195-9.